Chapter 1
Near-Infrared Light-Mediated Gold Nanoplatforms for Cancer Theranostics

Liming Wang, Yingying Xu, and Chunying Chen

Abstract In the past decade, great advances have been achieved for the biomedical application of gold (Au) nanostructures. Due to their unique physicochemical properties, Au nanostructures have been extensively explored for their use in cancer cell imaging, photothermal therapy, as well as drug/gene delivery. The facile control of synthesis and surface functionalization help the construction of multifunctional Au nanostructures for cancer diagnosis and treatment. Recently, Au nanostructure-based theranostic platforms have been extensively explored, and great advantages have been demonstrated. This chapter summarizes the recent progress of Au nanostructures as contrast agents for cancer imaging, as therapeutic composites for photothermal therapy and drug/gene delivery, and as multifunctional theranostic platform for cancer. The surface functionalization of Au nanostructures including noncovalent and covalent modification will also be discussed. We focus on the near-infrared (NIR) light-mediated cancer theranostics using Au nanostructures including Au nanoshells (AuNSs), Au nanorods (AuNRs), hollow Au nanospheres (HAuNSs), and Au nanocages (AuNCs).

Keywords Au nanostructures • Imaging • Photothermal therapy • Surface plasmon resonance • Cancer theranostics

L. Wang
CAS Key Laboratory for Biomedical Effects of Nanomaterials and Nanosafety, Institute of High Energy Physics, Chinese Academy of Sciences, Beijing 100049, China

Y. Xu • C. Chen (✉)
CAS Key Laboratory for Biomedical Effects of Nanomaterials and Nanosafety, National Center for Nanoscience and Technology of China, Beijing 100190, China
e-mail: chenchy@nanoctr.cn

1.1 Introduction

At present, cancer remains one of the major causes of human death in the world. Traditional cancer treatments, including surgery, chemotherapy, and radiotherapy, usually fail to radical cure because of the recurrence and metastasis of cancer. Chemotherapy, one of the most commonly used cancer treatments, has contributed greatly to reductions in cancer mortality. However, chemotherapeutic agents often cause adverse effects such as liver and kidney damage, hair loss, nausea, and cardiac toxicity [1–3]. These systemic hazards are generally due to the lack of drug specificity toward tumorigenic cells [4]. What's more, chemotherapy usually leads to drug resistance and causes treatment failure [5]. Therefore, there is an urgent need for the development of novel anticancer strategy.

Over the past decade, nanostructure-based cancer therapy and diagnosis have been largely explored. Among them, various types of Au nanostructures have been synthesized by scientists with tunable size and shapes (Fig. 1.1) [6–16]. These gold (Au) nanostructures are promising candidates for cancer theranostics because of their intrinsic physicochemical properties [17, 18]. Several unique features make Au nanostructures particularly suitable for cancer treatment and diagnosis. First, the small size of Au nanostructures enables them to preferentially accumulate at tumor sites either via passive targeting (i.e., the enhanced permeability and retention effect) or active targeting facilitated by tumor-targeting ligands conjugation. Second, the near-infrared (NIR, 650–900 nm) light absorption and scattering of Au nanostructures makes them excellent candidates as contrast agents for NIR imaging such as light scattering imaging, two-photon luminescence imaging, and photoacoustic tomography. Third, efficient light absorption and rapid heat conversion make Au nanostructures efficient photothermal conducting agents used in cancer photothermal ablation therapy. Last, the facile surface chemistry of Au nanostructures eases the simultaneous delivery of drugs, ligands, or imaging contrast agents, which enables the design of multifunctional theranostic nanoplatforms.

In this chapter, we review the recent progress on the NIR light-mediated Au nanoplatforms for cancer theranostics. We first summarize the recent progress on Au nanostructures used for NIR light-triggered optical imaging for cancer and then the hyperthermia therapy of cancer with Au nanostructures by the means of their photothermal effects. The functionalization of Au nanostructures including noncovalent and covalent chemical modification will also be discussed. We emphasize on the researches of NIR light-mediated theranostics application of Au nanoshells (AuNSs), Au nanorods (AuNRs), hollow Au nanospheres (HAuNSs), and Au nanocages (AuNCs).

1.2 Near-Infrared Light-Mediated Cancer Imaging by Au Nanostructures

One of the most dramatic and useful properties distinguishing nanoscale Au from its bulk form is the interaction between gold and light. When an Au nanoparticle is irradiated with light, strong absorption and/or scattering will occur at specific
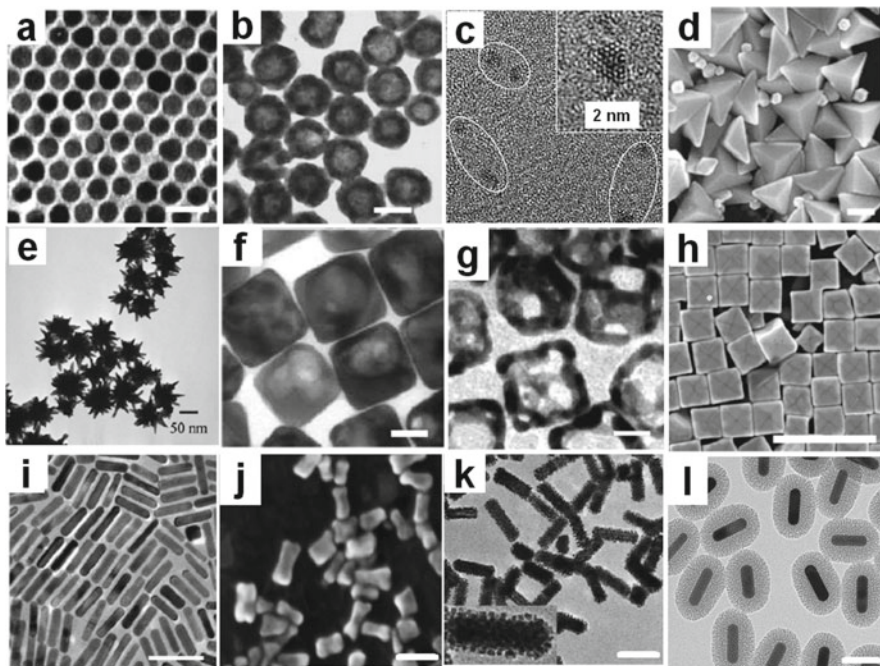
Fig. 1.1 Au nanomaterials of different shapes with potential biomedical use. (**a**) Au nanospheres (Reprinted with permission from ref. [6]. Copyright 2003, American Chemical Society). (**b**) Hollow Au nanospheres (Reprinted with permission from ref. [7]. Copyright 2005, American Chemical Society). (**c**) Au nanoclusters (Reprinted with permission from ref. [12]. Copyright 2011, American Chemical Society). (**d**) Au obtuse triangular bipyramids (Reprinted with permission from ref. [15]. Copyright 2011, American Chemical Society). (**e**) Au stars (Reprinted with permission from ref. [16]. Copyright 2012, Royal Society of Chemistry). (**f**) Au nanoboxes and (**g**) Au nanocages (Reprinted with permission from ref. [9]. Copyright 2007, American Chemical Society). (**h**) Au nanocubes (Reprinted with permission from ref. [10]. Copyright 2010, American Chemical Society). (**i**) Au nanorods (Reprinted with permission from ref. [11]. Copyright 2010, Elsevier Ltd.) (**j**) Au dog bones (Reprinted with permission from ref. [8]. Copyright 2006, John Wiley & Sons, Inc.). (**k**) Au@Pt nanorods with Pt nanodots (Reprinted with permission from ref. [13]. Copyright 2011, Elsevier Ltd.). (**l**) Mesoporous silica-coated Au nanorods (Reprinted with permission from ref. [14]. Copyright 2014, John Wiley & Sons, Inc.) Except of Fig. 1.1c, *scale bar* in all figures indicates 50 nm

resonant wavelength, which is known as localized surface plasmon resonance (LSPR). This phenomenon has been used for hundreds of years to give a brilliant color to stained glass and decorative artworks. However, the systematic study only began until 1857, when Michael Faraday demonstrated the synthesis of Au colloids in an aqueous medium and attributed the bright colors of the solutions to colloidal Au [19]. Then in 1908, by solving Maxwell's electromagnetic equation, Mie et al. attributed the intense colors in Faraday's Au solution to the absorption and scattering of light by Au nanospheres present in the solution [20]. John Turkevich pioneered a robust and simple synthesis method in 1951 [21]. Based on these studies, researchers developed novel strategies to exploit the unique physicochemical

properties and application of Au nanostructures [22–24]. By utilizing their optical properties, Au nanostructures have been extensively investigated for biomedical applications including biosensing, imaging, and cancer theranostics in recent years [25–28].

The frequency and cross section of LSPR absorption depend greatly on the size, shape, morphology, and dielectric environment of the Au nanostructures [29, 30]. For Au spherical nanoparticles (AuNSs), the LSPR absorption is at about 520 nm, and the peak wavelength varies slightly depending on the size and the embedding medium [29]. However, Au nanostructures such as nanoshells, nanorods, hollow nanospheres, and nanocages exhibit well-defined LSPR absorption features from the visible to the NIR region [31]. The optical properties of Au nanostructures enable their application as novel imaging and sensing probes. Due to the sensitivity of a nanostructure's LSPR to its surrounding environment, Au nanostructures have been developed as biosensors based on the shift of the LSPR for the detection of the local refractive index/dielectric constant of the environment surrounding the Au nanostructures [32].

Besides as biosensors, Au nanostructures with LSPR in the NIR region are also developed as novel imaging probes due to their interesting optical properties [33, 34]. Au nanostructures are especially attractive for their highly efficient absorption in the NIR region, a spectral window minimally absorbed by skin and tissue, which permits photons to penetrate biological tissues with relatively high transitivity. Au nanostructures have been employed as contrast agents for cancer imaging by using several imaging tools including dark-field microscope, two-photon luminescence (TPL), photoacoustic tomography (PAT), X-ray computed tomography (CT), optical coherence tomography (OCT), and surface-enhanced Raman scattering (SERS).

1.2.1   Dark-Field Microscopy

Au nanostructures exhibit enhanced Rayleigh scattering originating from their LSPR, which is heavily dependent on the nanostructure size and shape [35, 36]. Dark-field microscopic imaging is based on the intense light scattering ability of Au nanostructures [37]. The transmitted light is blocked, and scattered light is collected, showing bright scattering particles against a dark background. Compared to fluorescent dye molecules, the scattering cross sections of Au nanostructures give stronger photon intensity by more than four to five orders of magnitude [38]. Therefore, high-contrast images are attainable if the Au nanostructures accumulate within cancer cells by passive or active targeting.

Sokolov et al. functionalized AuNPs with the anti-epidermal growth factor receptor (EGFR) antibodies and observed bright light emission under dark-field monochromatic light illumination inside cervical cancer cell line SiHa, which overexpressed EGFR on the cell membrane. However, AuNPs functionalized with bovine serum albumin were not observed in the cell, which illustrated the necessity of EGFR-mediated targeting for cancer cell imaging [39]. El-Sayed et al. compared

the cellular binding and uptake of anti-EGFR conjugated AuNPs in nonmalignant malignant epithelial cell lines by dark-field imaging [40]. After incubation with anti-EFGR conjugated AuNPs, cancerous cells exhibited stronger light scattering than healthy cells when imaged using a dark-field microscopy, which demonstrated the great sensitivity of using dark-field light scattering to identify cancerous cells. Scattering from AuNPs has also been used for tracking dynamics of cancer cell mitosis and cell division [41].

Dark-field imaging has also enabled visualization of Au nanorods (AuNRs)-mediated cancer cell targeting and cellular localization [42, 43]. Huang et al. also observed strong light scattering from AuNRs in the NIR region [44]. They conjugated AuNRs with anti-EGFR antibodies to target two malignant epithelial cell lines, human oral squamous carcinomas HSC and HOC. The conjugate selectively accumulated in the malignant cell lines but not in a benign cell line HaCat (Fig. 1.2a, b). Oyelere et al. used the enhanced light scattering in a dark-field arrangement to identify nuclear localization of AuNRs after conjugation with nuclear localizing sequence (NLS) peptides [45]. Although the peptide-conjugated AuNRs were distributed into both nucleus and cytoplasm in either normal or cancer cells, the AuNRs were more concentrated in the nucleus of the cancer cells (Fig. 1.2c, d). By using
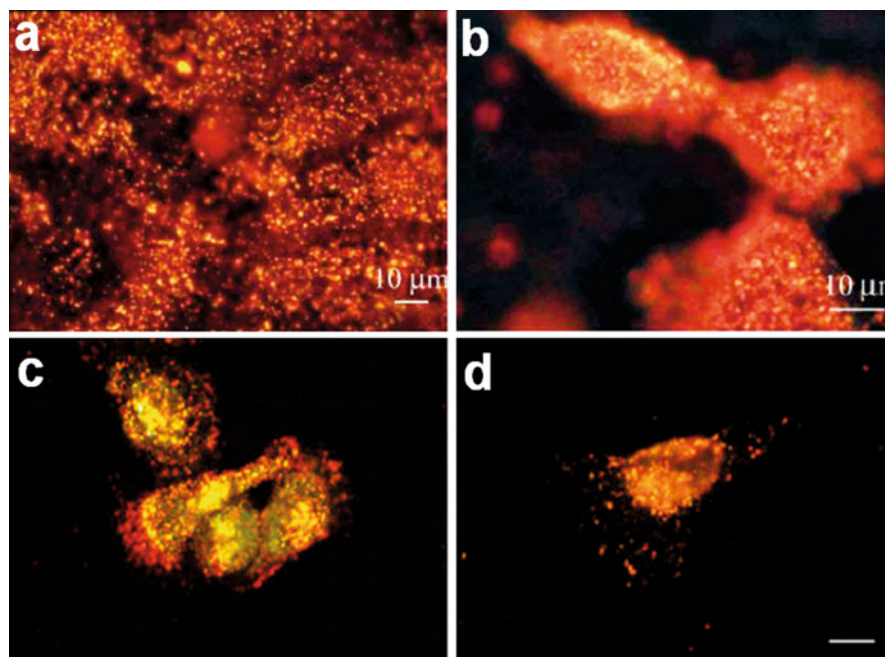

Fig. 1.2 Images of intracellular AuNRs. (**a**, **b**) Light scattering images of anti-EGFR-conjugated AuNRs after incubation with HaCaT nonmalignant cells (**a**) and HSC malignant cells for 30 min at room temperature (Reprinted with permission from ref. [44]. Copyright 2006, American Chemical Society). (**c**, **d**) HaCat normal cells (**c**) and HSC cancer cells (**d**) treated with nuclear localizing sequence (NLS) peptide-conjugated AuNRs. *Scale bar*: 10 μm (Reprinted with permission from ref. [45]. Copyright 2007, American Chemical Society)

dark-field microscopy and electron microscopy, Ding et al. studied the uptake and distribution of transferrin (Tf)-conjugated AuNRs in HeLa cells, which overexpressed the transferrin receptor (TfR) [46]. Minimal cellular uptake was observed with untargeted AuNRs compared to the conjugated AuNRs, which demonstrated receptor-mediated uptake of AuNRs into HeLa cells. Dark-field imaging has also been used for real-time tracking of AuNRs-induced DNA damage, causing cytokinesis arrest and apoptosis in cancer cells [47].

1.2.2 Two-Photon Luminescence (TPL)

Photoluminescence from Au nanostructures has drawn extensive interest in the past decade due to their bright, non-blinking, and stable emission. TPL of Au nanostructures exhibit increased light-penetration depth, submicron spatial resolution, low background fluorescence, and reduced photodamage to living tissues [48, 49]. Two-photon absorption occurs when Au nanostructures are excited with a femtosecond pulsed-NIR laser resonant with the surface plasmon energy. TPL is able to produce very strong signals under NIR laser excitation, even allowing single nanoparticle to be detected [50].

AuNRs, AuNSs, AuNCs, Au nanostars, and other nanostructures have been extensively exploited as TPL contrast agents. For instance, Durr et al. studied the capability of TPL imaging in a 3D tissue model using anti-EGFR antibody-conjugated AuNRs to target cancer cells embedded in the collagen matrices. The TPL signals of AuNRs are three orders of magnitude stronger than the autofluorescence from the surrounding tissues. These results demonstrated that AuNRs have strong signal, resistance to photobleaching, and good chemical stability and can serve as attractive contrast agent for TPL imaging of cancers [51]. Anti-EGFR antibody-conjugated AuNRs were also investigated for their effective binding both in A431, human squamous carcinoma cell line cells, in vitro and subcutaneous xenografts of A431 from Swiss nu/nu mice in vivo by using TPL imaging [52]. Tong et al. studied the targeting of folate-conjugated AuNRs and photo-induced injury to KB cancer cells and NIH-3T3 normal fibroblasts using TPL imaging. The localization of AuNRs after different incubation time was visualized, illustrating ligand-receptor binding-mediated endocytosis [53] (Fig. 1.3a–c). Selective targeting and internalization of chitosan oligosaccharide-modified AuNRs were visualized via TPL imaging in human oral adenosquamous carcinoma cell line CAL 27.

Further in vivo studies performed via NIR laser irradiation revealed similar targeting of the AuNRs conjugates in CAL 27 xenograft tumors [54]. By using fluorescence lifetime imaging microscopy (FLIM), which provides images with better contrast and sensitivity than intensity imaging, Zhang et al. studied the imaging of AuNRs in Madin-Darby canine kidney (MDCK) cells. They demonstrated that the characteristic fluorescence lifetime of AuNRs was less than 100 ps and could be used to distinguish AuNRs from other fluorescent labels and endogenous fluorophores in lifetime imaging [55]. As shown in Fig. 1.4a–c, AuNRs have the maximal
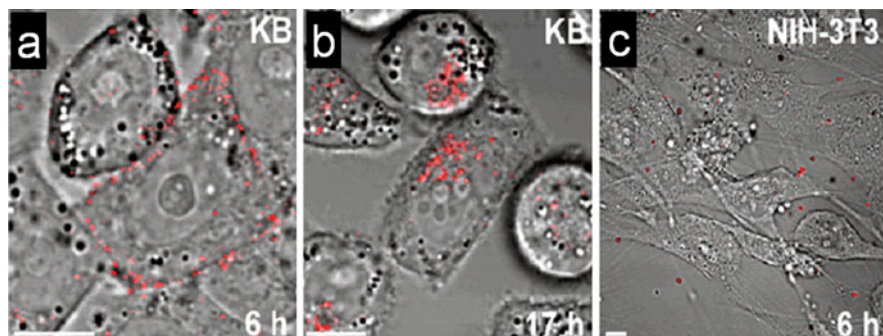
Fig. 1.3 (**a–c**) Targeted adsorption and uptake of folate-conjugated AuNRs (F-AuNRs, *red*) by KB cells overexpressing folate receptors. (**a**) A high density of F-AuNRs was observed on the surface of KB cells after 6 h incubation at 37 °C. (**b**) F-AuNRs were internalized into KB cells and delivered to the perinuclear region after 17 h incubation. (**c**) No binding was observed of F-AuNRs to NIH-3T3 cells, which express folate receptors at a low level. *Scale bar* = 10 μm (Reprinted with permission from ref. [53]. Copyright 2007, John Wiley & Sons, Inc.)
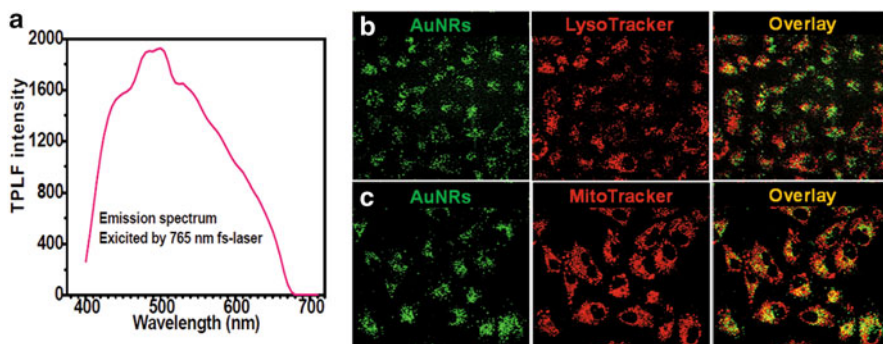

Fig. 1.4 Two-photon luminescence imaging of AuNRs and Au nanoshells in vitro and in vivo. (**a**) Luminescence emission spectrum of AuNRs when excited by two-photon laser at an optical wavelength of 765 nm, which is the LSPR maximum of these AuNRs (Reprinted with permission from ref. [14]. Copyright 2014, John Wiley & Sons, Inc.). (**b, c**) TPL images of serum protein-adsorbed CTAB-capped AuNRs with the organelles of human lung cancer cell line (A549). The *green fluorescence* indicates the AuNRs and the *red color* indicates the lysosomes (**b**) or the mitochondria (**c**). (Reprinted with permission from ref. [56]. Copyright 2011, American Chemical Society)

LSPR absorption, enabling TPL imaging of AuNRs inside cells. Based on TEM and TPL images, Wang et al. observed that CTAB-capped AuNRs can target the mitochondria of human lung cancer A549 cells and kill them efficiently. These AuNRs have a less storage at the lysosomes in normal human bronchiolar epithelial cell lines compared to cancer cells, which cause negligible effects on cell viability [56].

Besides AuNRs, Au nanostars have also been used as TPL contrast agents. Au nanostars functionalized with wheat-germ agglutinin have been utilized to image the cellular uptake in breast cancer cells, as well as the circulation in the vasculature in vivo in mouse models [57].

AuNSs [49, 58] and AuNCs [59] have also been extensively exploited as TPL contrast agents. The injected AuNS into a Balb/c mouse with subcutaneous tumors can clearly show the tumor and blood vessel structure based on in vivo TPL imaging [47]. AuNSs could be observed even as single nanoshell particles in blood vessels and generate optical contrast for blood vessel structure using TPL microscopy, which enable the tracking of AuNSs in vivo [60]. TPL of AuNCs has been used to examine the uptake of antibody-conjugated and PEGylated AuNCs by U87MGwtEGFR cells. Antibody-conjugated AuNCs could be attached to the surface of the cells and internalized into the cells via receptor-mediated endocytosis [61].

1.2.3 Photoacoustic Tomography (PAT)

PAT is a new combinational imaging method which detects the ultrasonic waves thermoelastically converted by photons in tissue through the photoacoustic effect. It requires a nanosecond-pulsed laser as an excitation source to stimulate thermal and acoustic responses. And acoustic waves are detected by an ultrasonic transducer to subsequently form a high-resolution tomographic image. The materials used for PAT imaging need to be able to absorb light and convert it into heat efficiently. Au nanostructures are ideal candidates for PAT imaging for their LSPR-based light absorption.

Au nanostructure-mediated PAT has been realized with AuNPs [62], AuNRs [63], and AuNSs [64]. Mallidi et al. performed multiwavelength PAT on gelatin implants in ex vivo mouse tissue containing anti-EGFR-labeled AuNPs targeted to epithelial carcinoma cells. High sensitivity and selectivity in the photoacoustic signal were achieved with the molecularly targeted AuNPs compared to nontargeted AuNPs and a NIR-absorbing dye [65]. Kim et al. investigated AuNCs conjugated with melanocyte-stimulating hormone for molecular PAT of melanomas in vivo. Compared to unconjugated AuNCs, a 300 % enhancement of contrast was achieved compared to the control PEGylated AuNCs [66]. AuNC-enhanced PAT was also used for sentinel lymph node mapping in a rat model, which provided valuable information for metastatic cancer staging [67]. Due to the tunable optical absorption property of AuNRs, multiple selective targeting on oral cancer cells both in vitro and in vivo can be observed according to PAT imaging [68]. The contour of the tumor region was sharply visualized in fusion images acquired from PAT signals with antibody-mediated targeting, while imaging was not obtained at the tumor sites of mice injected with AuNRs alone. Intracellular AuNRs imaging was reported by Yang et al. Using a homemade photoacoustic microscope, time-dependent cellular uptake and distribution of AuNRs in human breast adenocarcinoma cell line were
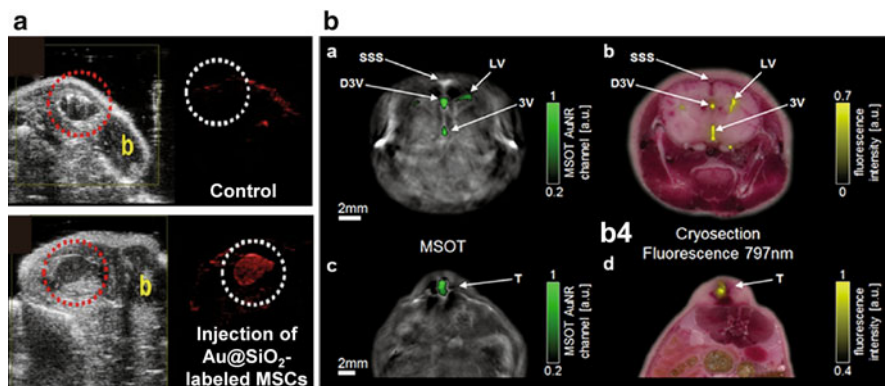
Fig. 1.5 (**a**) In vivo backscatter mode ultrasound (*gray scale*) and PAT (*red*) images of the intramuscular injection of a negative control (No Au@SiO$_2$, no cells) and Au@SiO$_2$-labeled mesenchymal stem cells in 50 % matrigel/PBS into hind limb muscle of an athymic mouse. "*b*" indicates bone and the *red-dashed circle* highlights the injection (Reprinted with permission from ref. [70]. Copyright 2012, American Chemical Society). (**b**) PAT and fluorescence imaging of NIR-liposome-AuNR hybrids in (*b1, b2*) the brain and (*b3, b4*) tumor tissue. (*b1, b2*) PAT image after injection of 5 μL of the hybrid into the dorsal third ventricle (D3V) of the mouse brain. (*b3, b4*) Images are obtained 6 h after injection of the hybrid into an HT29 xenograft (T). (*b2, b4*) Corresponding images of cryosectioned brain tissue and tumor tissue. *Abbreviations*: *SSS* superior sagital sinus, *LV* lateral ventricle, *3V* third ventricle. The *green overlay* shows PAT signal from the AuNRs. The *grayscale* background is an optoacoustic image taken at 900 nm (Reprinted with permission from ref. [74]. Copyright 2012, American Chemical Society)

successfully monitored [69]. Recently, mesoporous silica-coated AuNRs (Au@SiO$_2$)-based PAT imaging has been investigated. Jokerst et al. reported PAT imaging of mesenchymal stem cells in living mice via Au@SiO$_2$ [70]. They monitored mesenchymal stem cells in living mice via Au@SiO2 and found that the silica layer enhanced the photoacoustic signal of AuNRs (Fig. 1.5a). These studies demonstrate that Au nanostructures have great potential for contrast enhancement of PAT imaging. With the development in rational design and preparation of unique nanostructures with targeting capacity, the desired spatiotemporal resolution of PAT will be realized.

1.2.4   X-ray Computed Tomography (CT)

X-ray CT is an imaging technique based on the different absorption of X-ray by different compositions of the tissue. Small iodinated molecules are generally used as contrast agents in X-ray CT due to their high X-ray absorption coefficient. However, these contrast agents generally experience rapid renal excretion and allow very short time imaging.

Recently, Au nanostructures have attracted much attention as CT contrast agents for the detection of cells and tissues due to their strong X-ray absorption ability. von Maltzahn et al. developed a PEG-coated AuNRs which exhibited twofold higher X-ray absorption than a clinical iodine contrast agent [71]. By using X-ray CT, the biodistribution and accumulation of PEG-AuNRs were monitored. With four-dimensional biodistribution-based heat transfer simulations, they achieved complete tumor regression in mice treated with PEG-AuNRs following computationally tailored irradiation. Luo et al. reported $Au@SiO_2$ loading the cyaninedye indocyanine green (ICG) for the dual modality of X-ray CT and fluorescence imaging [72]. They demonstrated that $Au@SiO_2$ could enhance the CT contrast significantly and multiplexed images could be obtained by this dual-mode imaging. By conjugating $Au@SiO_2$ with the tumor-targeting molecule folic acid, the same group used X-ray CT to monitor the tumor-targeting ability of folic acid-conjugated $Au@SiO_2$ [73].

1.2.5   Optical Coherence Tomography (OCT)

OCT is a newly developed optical imaging technique which can capture three-dimensional cellular and subcellular tissue morphology using the coherence-gated detection of scattered light. OCT is based on low-coherence interferometry, in which tissue is illuminated with light of low coherence in NIR region, and the detection is based on coherence matching between the incident and reflected beams. Au nanostructures have been used as OCT contrast-enhancing agents due to their intense optical absorption or scattering ability (Fig. 1.5b) [70, 74].

Zagaynova et al. employed NIR-resonant AuNSs as OCT contrast agents for deep tissue (up to 2 mm depth) imaging of rabbit epidermal tissue. AuNSs enhanced the OCT signal of the different regions of the dermis with high spatiotemporal resolution [75]. AuNRs-mediated OCT contrast enhancement was also reported in human breast tissue samples [76]. AuNRs significantly enhance the tissue depth for the detection of OCT signals. In another work, AuNRs uptake in sentinel lymph node (SLN) of mice in situ was monitored by OCT imaging [77]. Improved resolution was obtained with AuNRs-mediated OCT system compared to conventional scattering OCT. Kim et al. employed AuNPs conjugated with anti-EGFR antibodies to enhance OCT contrast of oral dysplasia in a hamster model in vivo [78]. By using microneedles and ultrasound, the distribution and penetration depth of AuNPs into skin tissue were improved, and obvious differences could be observed between micro-morphologies of the carcinogen-treated and untreated epithelial tissues with OCT imaging. This study demonstrates an effective approach to improve the penetration and transportation of nanoparticles for OCT contrast enhancement for the early diagnosis of cancer.

1.2.6 Surface-Enhanced Raman Scattering (SERS)

SERS was first reported in the late 1970s. When a molecule is absorbed on rough metal surfaces or nanostructures, Raman signal enhancement occurs and results in up to 10^{14} enhancement compared to traditional Raman scattering [79]. Although the exact mechanism that results in surface enhancement has not been completely elucidated, there are two generally accepted mechanisms, electromagnetic (EM) and chemical enhancement (CE). The EM mechanism requires the excitation of the LSPR of a surface, which leads to an increase in the local EM field. The CE involves charge transfer interactions between the surface and the molecules adsorbed on it [80]. The EM is the dominant mode of enhancement between the two mechanisms.

Due to the strong LSPR, Au nanostructures can enhance the Raman signals of the molecules absorbed on their surface by many orders of magnitude. The Au nanostructure-based SERS enable ultrasensitive biomarkers detection, SERS-based imaging, and image-guided therapy [81–85]. Huang et al. reported label-free SERS for cancer identification using tumor-targeting AuNRs [86]. They recorded the SERS spectra in cancerous and healthy cell lines incubated with anti-EGFR antibody-conjugated AuNRs. The signals of SERS spectra obtained from cancerous cells were greatly enhanced. Kang et al. utilized AuNPs to obtain SERS spectra of living HSC-3 cells throughout the entire life cycle [87]. AuNPs were functionalized with nuclear localizing sequence (NLS) peptides to facilitate AuNPs nuclear localization. The different phases of cell cycle were simultaneously recorded by Rayleigh images and Raman spectra in real time, and the phase-specific SERS bands could be identified by the observed Raman DNA and protein peaks.

Dual modality imaging has been recently investigated with iron oxide-Au heteronanostructures functionalized with a Raman-active dye molecule, DTTC (AuMN-DTTC). The probe can be visualized both in silico and in vivo in deep tissue in live animals. After injecting the nanostructures deep into the gluteal muscle, MRI-SERS imaging was obtained, and Au nanostructure-mediated Raman enhancement was clearly observed [88] (Fig. 1.6). Wang et al. labeled AuNPs with epidermal growth factor (EGF) peptide for circulating tumor cells (CTCs) targeting. CTCs are cells circulating in the bloodstream which have been shed from a primary tumor. CTCs are responsible for the development of tumor metastasis. By using SERS, they successfully identified CTCs from blood samples of patients with different stages of squamous cell carcinoma of the head and neck, with a range of 1 to 720 CTCs per milliliter of whole blood [89]. These results demonstrate that Au nanostructure-based SERS imaging may provide a promising platform for multimodal imaging and imaging-guided cancer therapy.
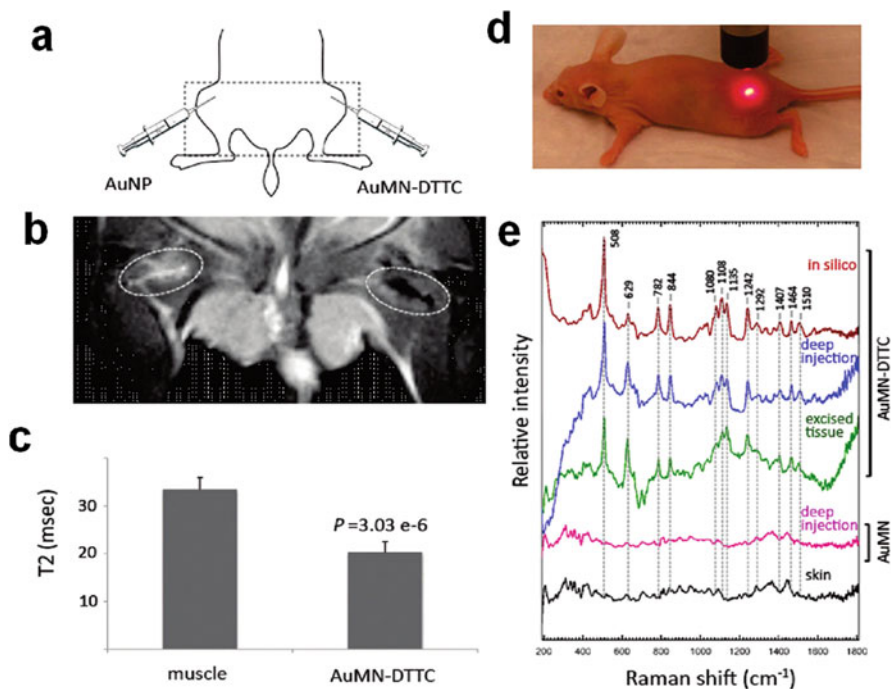
Fig. 1.6 MRI and Raman spectroscopy of AuNPs complexed with dextran-coated superparamagnetic iron oxide nanoparticles (AuMN-DTTC) in vivo. (**a**) A schematic of the probe injection setup. The experimental AuMN-DTTC probe was injected in the deep right gluteal muscle. A control probe was injected in the contralateral muscle. (**b**) In vivo T2-weighted MR image of a mouse-injected intramuscularly (i.m.) with AuMN-DTTC and the control probe, AuNPs. Notable loss of signal intensity associated with the site of the AuMN-DTTC injection indicated the suitability of the probe as an in vivo MRI contrast agent. (**c**) Calculated T2 values based on multiecho T2-weighted MRI. The T2 relaxation time of AuMN-DTTC was significantly lower than both noninjected muscle and muscle injected with AuNPs ($n=3$; Student's t test; $p<0.05$). (**d**) A photograph demonstrating the Raman spectroscopy experimental setup. (**e**) In vivo Raman spectra of a mouse-injected i.m. with AuMN-DTTC and the control probe, AuMN. The in vivo Raman spectrum of muscle injected with AuMN-DTTC has a clear SERS signature, which is indistinguishable from that obtained ex vivo and in silico and is absent in skin tissue and in muscle injected with the control probe (Reprinted with permission from ref. [88]. Copyright 2011, American Chemical Society)

1.3 Cancer Photothermal Therapy by Au Nanostructures

One of the major therapeutic applications of Au nanostructures is to treat cancers as photothermal therapy agents. Au nanostructures can efficiently absorb light followed by rapid heat conversion, which makes them suitable candidates for cancer photothermal therapy. Additionally, the absorption wavelength of Au nanostructures can be easily tuned to the NIR region by changing their size and shape, which allows high-depth cancer photothermal therapy in tissues.

The early research about Au nanostructure for photothermal therapy was spherical AuNPs reported by Lin and co-workers in 2003. They conjugated AuNPs with IgG to target the CD8 receptor on the peripheral blood lymphocyte cells. After irradiation with a nanosecond-pulsed visible laser, they found that 95 % of cells containing as few as ~500 nanoparticles per cell were killed (versus 5–8 % in a control treatment) [90]. After that, El-Sayed group reported selective cancer photo-thermal therapy using spherical AuNPs conjugated to anti-EGFR antibodies [91]. The tumor-targeting AuNPs could specifically accumulate in HSC and HOC human oral squamous cell lines while not in a benign cell line (HaCaT). Under the irradia-tion of a continuous wave argon ion laser at 514 nm, the two cancer cell lines were damaged by hyperthermia within 4 min at laser energy thresholds of 19 and 25 W/cm^2 respectively, which is much less than that of the benign cells (57 W/cm^2). The results indicated a selective photothermal damage of cancer cells.

The absorption and scattering coefficients AuNRs are an order of magnitude higher than those of AuNPs and AuNSs. Therefore, the applications of AuNRs for cancer photothermal therapy have been extensively investigated in the past decade. Tong et al. studied the mechanism of hyperthermia-induced cell necrosis by folate-conjugated AuNRs [53]. They observed a rapid increase in intracellular calcium induced by photothermal therapy. Additionally, disruption of the actin-network and the formation of membrane blebs were observed. The authors found that the dam-age to the cells was more effective when AuNRs were adsorbed to the cell surface prior to uptake. They thus attributed the cell necrosis to the disruption of the plasma membrane. To avoid photothermal damage to the healthy cells, Rejiya et al. conju-gated AuNRs with anti-EGFR antibody [92]. The targeting efficiency of anti-EGFR-AuNRs to tumor was evaluated by inductively coupled plasma-atomic emission spectroscopy (ICP-AES) and immunofluorescence studies, which showed much higher cellular uptake of anti-EGFR-AuNRs by A431 cells compared to unconjugated AuNRs. With laser irradiation, anti-EGFR-AuNRs treatment induced 92 % mortality of the carcinoma cells, while only 9 % cell death was induced by unconjugated AuNRs treatment. The author also demonstrated that anti-EGFR-AuNRs selectively induced cancer cell apoptosis through ROS-mediated mitochon-drial pathway under low power laser exposure. By using PEG-conjugated AuNRs, Dickerson et al. studied the cancer photothermal therapy in vivo [93]. The nanopar-ticles were injected intravenously or directly to subcutaneous squamous cell carci-noma xenografts grown in nude (nu/nu) mice. Suppression of tumor growth was observed by NIR laser- induced hyperthermia after intravenous or direct injection. Li et al. investigated the cancer photothermal therapy of RGD-conjugated dendrimer-modified AuNRs (RGD-AuNRs) in vivo [94]. RGD-AuNRs could specifically tar-get tumor cells overexpressing $\alpha_v\beta_3$ integrin both in vitro and in vivo. The selective destructive effects on solid tumors under NIR laser irradiation were therefore achieved. Our group has designed mesoporous silica-coated AuNRs ($Au@SiO_2$) loaded with doxorubicin (DOX) for simultaneous TPL imaging, photothermal ther-apy, and drug delivery in cancer cells [95]. NIR light-triggered drug release was realized for chemotherapy by low-intensity NIR laser irradiation, while higher irra-diation intensity also induced obvious hyperthermia effects of the AuNRs for direct

cell killing. Synergistic effect was achieved for combined thermo-chemotherapy compared to hyperthermia or chemotherapy alone (Fig. 1.7).

Photothermal therapy of AuNSs has also been studied extensively to treat cancer, and the nanoshells are currently under FDA-trial. AuNSs exhibit similar optical properties to AuNPs, and the LSPR of AuNSs can be shifted to the NIR region, which is dependent on the relative thickness of Au shell to the core size [96]. Hirsh et al. first demonstrated that AuNSs as photothermal agents can be formulated with a dielectric silica core and an ultrathin Au shell [97]. Bernardi et al. conjugated AuNSs with antibodies against interleukin-13 receptor-alpha 2 (IL13Rα2) to target medulloblastoma and glioma human brain tumor cell lines [98]. The tumor-targeting AuNSs induced photothermal ablation in the two cell lines in vitro with high specificity and sensitivity. Day et al. reported in vivo photothermal therapy of glioma tumor models and demonstrated much longer survival rate of mice that were administered with nanoshells compared to that of mice with only laser treatment [99]. Combined cancer therapy has been reported by combining photothermal therapy and radiotherapy. AuNSs-mediated photothermal therapy can increase tumor vascular perfusion and reduces the resistance of the hypoxic region of tumors to radiotherapy [100].

These studies demonstrate the great potential of Au nanostructure-mediated hyperthermia in cancer therapy. Using the Au nanostructure-mediated photothermal therapy, multifunctional platforms could be constructed combining photothermal therapy with cancer imaging or other treatment strategies. In the past decade, Au nanostructures with unique geometrics have been explored for new diagnostic and therapeutic applications. The tunable geometric shapes endow Au nanostructures with unique LSPR effects, which make them highly potential both in cancer imaging and therapy. In addition, the easy functionalization of Au nanostructures endows them readily be adapted to various biomedical applications.

1.4   Functionalization of Au Nanostructures

One of the most advantageous properties of Au nanostructures in the biomedical field is their surface stability, which affords facile surface functionalization with various biological molecules. By noncovalent and covalent surface modification, specific biological targeting, imaging, and diagnostic molecules can be attached to Au nanostructures. Besides, the potentially toxic initial-stabilizing agents during the synthesis of Au nanostructures can be removed and replaced to improve their biocompatibility. For instance, AuNRs prepared by the wet chemical seed-mediated synthesis are coated with the surfactant of cetyltrimethylammonium bromide (CTAB), which makes the surface of AuNRs positively charged and prevents their aggregation. However, CTAB can cause cytotoxicity by disrupting the biomembrane integrity [11]. Noncovalent modifications include electrostatic interactions,
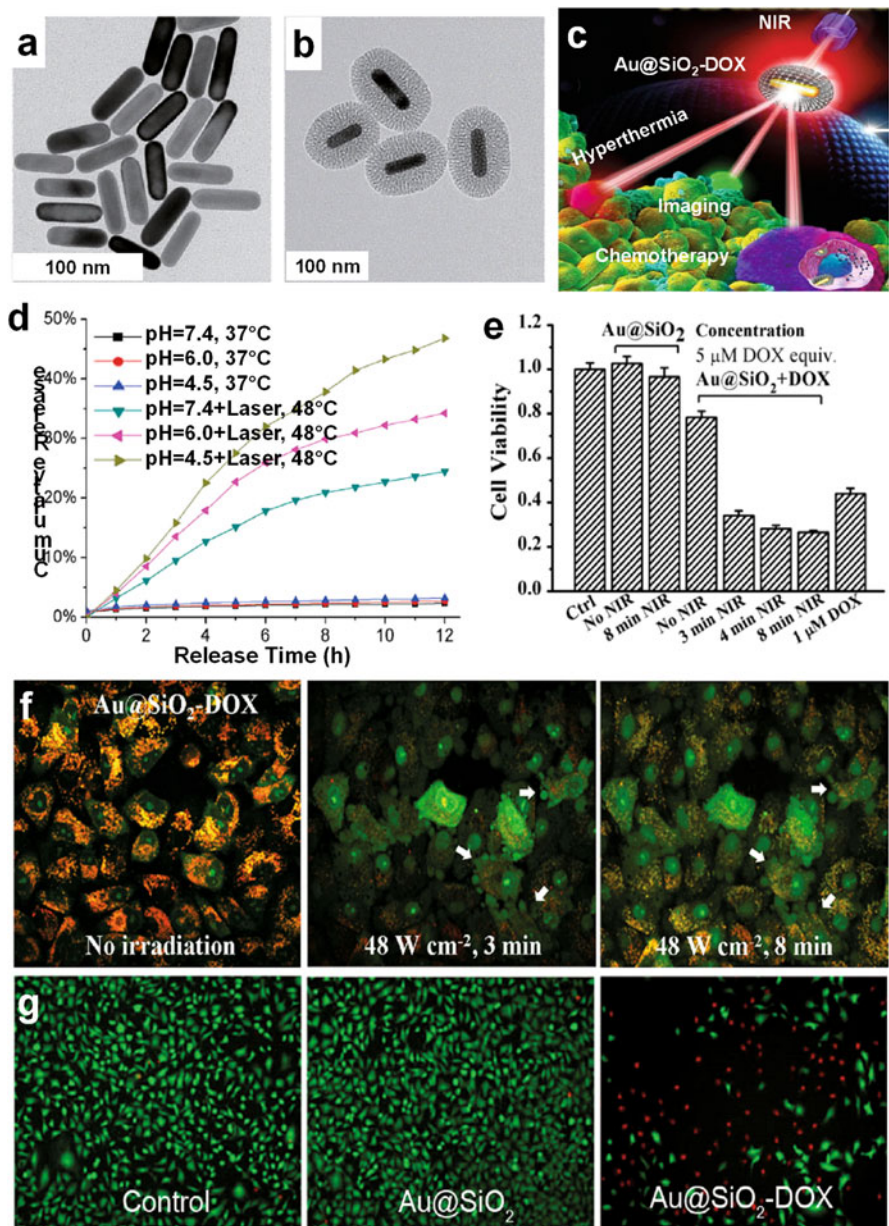
Fig. 1.7 TEM images of (**a**) AuNRs and (**b**) Au@SiO$_2$. (**c**) Schematic illustration of Au@SiO$_2$-DOX as a novel multifunctional theranostic platform to treat cancers. (**d**) DOX release profiles from Au@SiO$_2$-DOX at different pHs, with and without a 790 nm laser irradiation. (**e**) After 24 h uptake of Au@SiO$_2$ and Au@SiO$_2$–DOX, differences in viability of human lung cancer A549 cells irradiated by the laser for 3, 4, and 8 min, determined by CCK-8 assay. (**f**) Effects of NIR laser irradiation on the lysosomal membrane integrity determined by acridine orange (AO) staining. Au@SiO$_2$-DOX-treated cells are irradiated by a laser at 48 W/cm^2 for 0, 3, and 8 min. (**g**) Live-Dead staining of A549 cells 24 h postirradiation. A549 cells are treated with Au@SiO$_2$ or Au@SiO$_2$-DOX for 24 h and then radiated for 3 min using a laser at 20 W/cm^2 (Reprinted with permission from ref. [95]. Copyright 2012, John Wiley & Sons, Inc.)
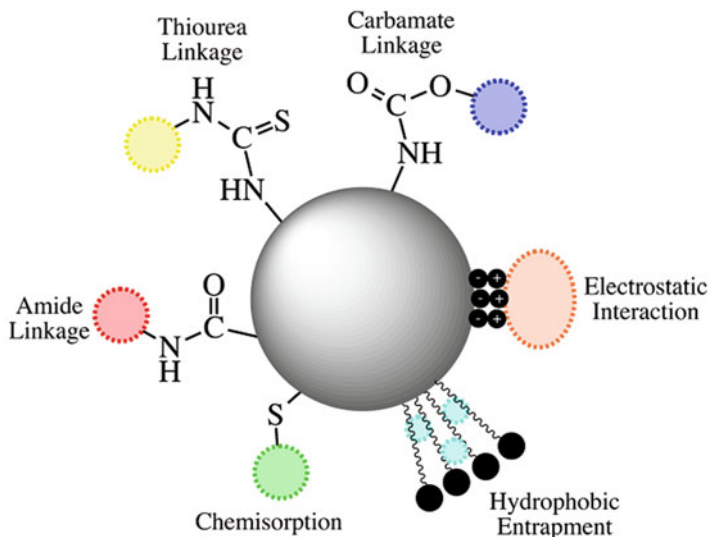
Fig. 1.8 Common surface functionalization strategies for Au nanostructures for use in biomedical applications (Reprinted with permission from ref. [33]. Copyright 2014, Springer-Verlag Berlin Heidelberg)

hydrophobic entrapment, and van der Waals force interactions, while covalent modifications utilize direct chemical attachment, linker molecules, or click chemistry (Fig. 1.8).

1.4.1 Noncovalent Functionalization

Noncovalent functionalization of Au nanostructures generally needs the assembly with a variety of superstructures and the inclusion of new functionalities, which can be realized by electrostatic attraction, antibody-antigen interaction, or DNA sequence recognition. Electrostatic interactions are common strategy to functionalize Au nanostructures to biomolecules, such as DNA, peptides, and antibodies. The interaction depends on the attraction between oppositely charged nanostructure and the biomolecule of interest. Since the biomolecule is not exposed to harsh chemical modifications, this functionalization could keep its native, active conformation. For instance, McIntosh et al. utilized electrostatic interaction to functionalize cationic Au clusters with DNA using the negatively charged phosphate backbone of DNA [101]. The stability of the DNA-functionalized Au clusters was verified by UV-Vis spectroscopy and dynamic light scattering (DLS). Huang et al. have also used this interaction to functionalize AuNPs and AuNRs with anti-EGFR antibodies to selectively target and photothermally ablate cancer cells [44, 86]. One widely used strategy for the surface modification of AuNRs is layer-by-layer electrostatic absorption,

which involves the sequential deposition of negatively and positively charged polyelectrolytes to the positively charged surface of AuNRs [102]. Negatively charged polyacrylic acid (PAA) and polystyrene sulfonate (PSS) are often used as a mild detergent and absorbent to remove CTAB, and then positively charged polyelectrolytes such as poly(diallyldimethyl-ammonium chloride) (PDDAC) or poly (allylamine hydrochloride) (PAH) will be absorbed on the surface of PAA/PSS-coated AuNRs. The deposition cycle can be repeated, and multilayered poly-electrolytes can be formed. Biological polyelectrolytes and proteins can also be deposited among the appropriate layer through electrostatic adsorption [103–105].

Hydrophobic entrapment is generally used for the loading of hydrophobic molecules. Kim et al. utilized the noncovalent interactions to load hydrophobic therapeutics tamoxifen and β-lapachone to AuNPs [106]. The AuNPs were functionalized with water-soluble zwitterionic ligands to form kinetically stable complexes with hydrophobic drugs and dyes. The complex mimicked micelle structures and facilitated the encapsulation of hydrophobic drugs in the hydrophobic pockets. Another noncovalent surface modification for AuNRs is to coat AuNRs with a mesoporous silica layer [107]. Mesoporous silica nanoparticles are ideal drug carriers with high surface area and large pore volume [108], which endow AuNRs excellent drug delivery system. Our group has developed Au@SiO$_2$ as a light-mediated multifunctional theranostic platform for cancer treatment [95, 109].

1.4.2   Covalent Functionalization

Covalent functionalization generally provides greater stability and reproducibility of the attached molecules compared to noncovalent functionalization. Au-thiol (Au-S) bonding chemistry is commonly utilized for the covalent surface modification of Au nanostructures. Thiolated biopolymers such as PEG have been extensively employed for the functionalization of Au nanostructures. Thiol-terminated PEG endows Au nanostructures high stabilities and improves their biocompatibilities. Additionally, PEG functionalization can avoid nonspecific binding of serum proteins when introduced into in vivo systems [110, 111].

Au-S bond formation has been used to attach oligonucleotides to the surfaces of Au nanostructures. Alivisatos and Mirkin have independently reported oligonucleotide functionalized AuNPs in 1996 [112, 113]. Then various biomedical applications have been explored by using this kind of functionalization, such as hepatitis C virus detection, intracellular gene regulation, and mercuric ion detection [114–116]. Tumor-targeting peptide RGD has also been conjugated to AuNPs and AuNRs surfaces through the Au-S bond [117, 118]. To promote nuclear localization, nuclear localizing sequence (NLS) peptide has also been conjugated to AuNPs and AuNRs via cysteine residues located within the peptides [45, 47]. Black et al. conjugated deltorphin, a high-affinity ligand for delta opioid receptor (deltaOR) to AuNRs through a thiolated PEG for specific targeting of cancer cells [119]. Some other

thiolated species have also been used for the surface functionalization of Au nanostructures, such as thiolated DNA for gene therapy. For instance, Yamashita et al. reported a controlled-release system of single-stranded DNA (ssDNA) triggered by the photothermal effect of AuNRs by modifying AuNRs with double-stranded DNA (dsDNA). When the dsDNA-modified AuNRs were irradiated by NIR light, the ssDNA could be released from AuNRs due to the photothermal effect [120].

Bifunctionalized linkers are generally used to covalently attach therapeutic drugs and biomolecules to nanostructures to reduce the possibility of structural changes, since it has been demonstrated that proteins that directly interact with the nanoparticle surface may undergo conformational changes and alter their biological activity [121]. By using a pH-sensitive hydrazone linker, Prabaharan et al. covalently attached DOX to the hydrophobic inner layer of the folic acid-conjugated amphiphilic AuNPs. The targeted DOX-conjugated AuNPs showed selective uptake and DOX release to breast cancer cells [122]. Qian et al. conjugated tumor-targeting antibodies, single-chain variable fragment (ScFv) antibodies, to AuNPs using heterobifunctional PEG linkers and EDC/NHS coupling [123]. Click chemistry has been utilized for Au nanostructures functionalization and related applications. By using click chemistry, Fischler et al. coupled azide-functionalized AuNPs to an alkyne-modified DNA duplex, to obtain a chain-like assembly of AuNPs on the DNA template [124]. Click chemistry-based assay has also been explored for quantitative detection of proteins. This assay has a broader linear range and good selectivity compared to conventional methods, which enables the analysis of total proteins in various sera and milk samples [125].

1.5 Au Nanoshells (AuNSs)

During the past decade, Au nanostructures have been extensively investigated for diagnostic agents and therapeutic actuators. Recently, researchers have begun to combine these two functionalities into a single nanoparticle to generate "theranostic" nanoplatform and realize simultaneous cancer diagnostics and therapy. Due to their unique optical properties and geometric structures, Au nanostructures can be used simultaneously as imaging probes, photothermal mediator, and drug delivery vehicles. Au nanostructure-based theranostic platforms have been extensively developed either by combining a single imaging modality and therapeutic modality or by integrating multimodality diagnostics with therapeutic functionalities.

As early as in a decade ago, the theranostic potential of AuNSs has been demonstrated with simultaneous dark-field imaging and photothermal therapy by Loo et al. [126, 127]. They first demonstrated the possibility of engineering AuNSs for combined imaging and therapy for cancer cells. Immunotargeted AuNSs nanoplatform for both detecting and thermally ablating human breast cancer cells that overexpress human epidermal growth factor receptor 2 (HER2) was designed. These theranostic AuNSs could provide scattering contrast for dark-field imaging and also sufficient absorption to enable effective photothermal therapy [127]. Dramatic contrast enhancement for optical coherence tomography (OCT) and effective photothermal

ablation of tumors in vivo have been reported by Gobin et al. [128]. PEG-modified AuNSs were injected intravenously in tumor-bearing mice, and significant accumulation of particles within the tumor tissue dramatically increased the NIR scattering and the OCT contrast. Meanwhile, photothermal ablation of the tumor significantly reduced the tumor size and prolonged the mice surviving rate. Lu et al. used PEG and $\alpha_v\beta_3$ integrin-targeted cyclic RGD peptide (c(KRGDf)-PEG)-modified hollow Au nanospheres (HAuNS) to track endothelial cells and glioma tumors in the mouse brains. With high target ability to tumor, the photothermal therapy is efficient to ablate the tumors and inhibit their growth (Fig. 1.9) [129].

Halas and Joshi synthesized theranostic immunotargeted AuNSs by encapsulating them in a thin silica epilayer doped with Fe_3O_4 nanocrystals and ICG molecules to target HER2 receptors in cancer cells [130, 131]. In this approach, the quantum yield of ICG increased from a mere ~1 % to nearly ~85 %, and the porous silica layer enabled rapid water diffusion, which enhanced the MRI relaxivity of the Fe_3O_4 nanocrystals. In the in vivo mouse model with breast cancer xenografts, the MRI and fluorescence imaging revealed that the maximum AuNSs accumulation in tumors occurs within 4 h of injection [132]. This theranostic nanoplatform enabled simultaneous active targeting of HER2 expressing cancer cells, diagnosis via dual modal MRI and near-infrared fluorescence, and photothermal therapy. AuNSs with hollow interior have been developed to facilitate drug delivery for dual modal cancer thermo-chemotherapy. AuNSs consist of a mesoporous silica nanorattle core and a thin outer Au shell (SN@AuNSs) fabricated by Liu et al. [133]. Anticancer drug docetaxel was loaded in SN@AuNSs, and a synergistic effect of chemotherapy and photothermal therapy both in vitro and in vivo was observed [133, 134]. Additionally, FITC labeling of the SN@AuNSs enabled the fluorescent imaging for their intracellular localization. Lee et al. developed DOX-loaded poly(ethylene glycol)-poly(lactic-co-glycolic acid)-Au half-shell nanoparticles (DOX-loaded PEG-PLGA-Au H-S NPs) to facilitate combined NIR fluorescent imaging and thermo-chemotherapy treatment in vivo [135]. Both intravenously and intratumorally injected NPs could be accumulated in the tumor region in A431 tumor-bearing mice, which was revealed by time-lapse in vivo fluorescence imaging. DOX could be rapidly released in the tumor region upon NIR light irradiation, and the combined thermo-chemotherapy resulted in complete destruction of the tumors without weight loss or recurrence of tumors.

Other imaging modalities including PET and ultrasound imaging have also been integrated with photothermal therapy in AuNSs. Xie et al. demonstrated that integrin $\alpha_v\beta_3$ targeting using cyclo-(RGDfK) peptide-conjugated AuNSs improved the nanoshells' accumulation in tumors. Meanwhile, increased degree of tumor necrosis indicated biological effectiveness of targeted AuNSs in the photothermal therapy application [136]. Core-shell nanoparticles composed of a superparamagnetic iron oxide (SPIO) core and an Au shell (SPIO@AuNS) were fabricated by Melancon et al. to investigate their multifunctional imaging and therapeutic capabilities [137]. In vivo, significant temperature elevations were revealed by both MRI and magnetic resonance temperature imaging when intratumorally injected with SPIO@AuNSs and irradiated with NIR light. SPIO@AuNS-mediated simultaneous MRI and photothermal therapy demonstrated the potential use of SPIO@AuNS for real-time
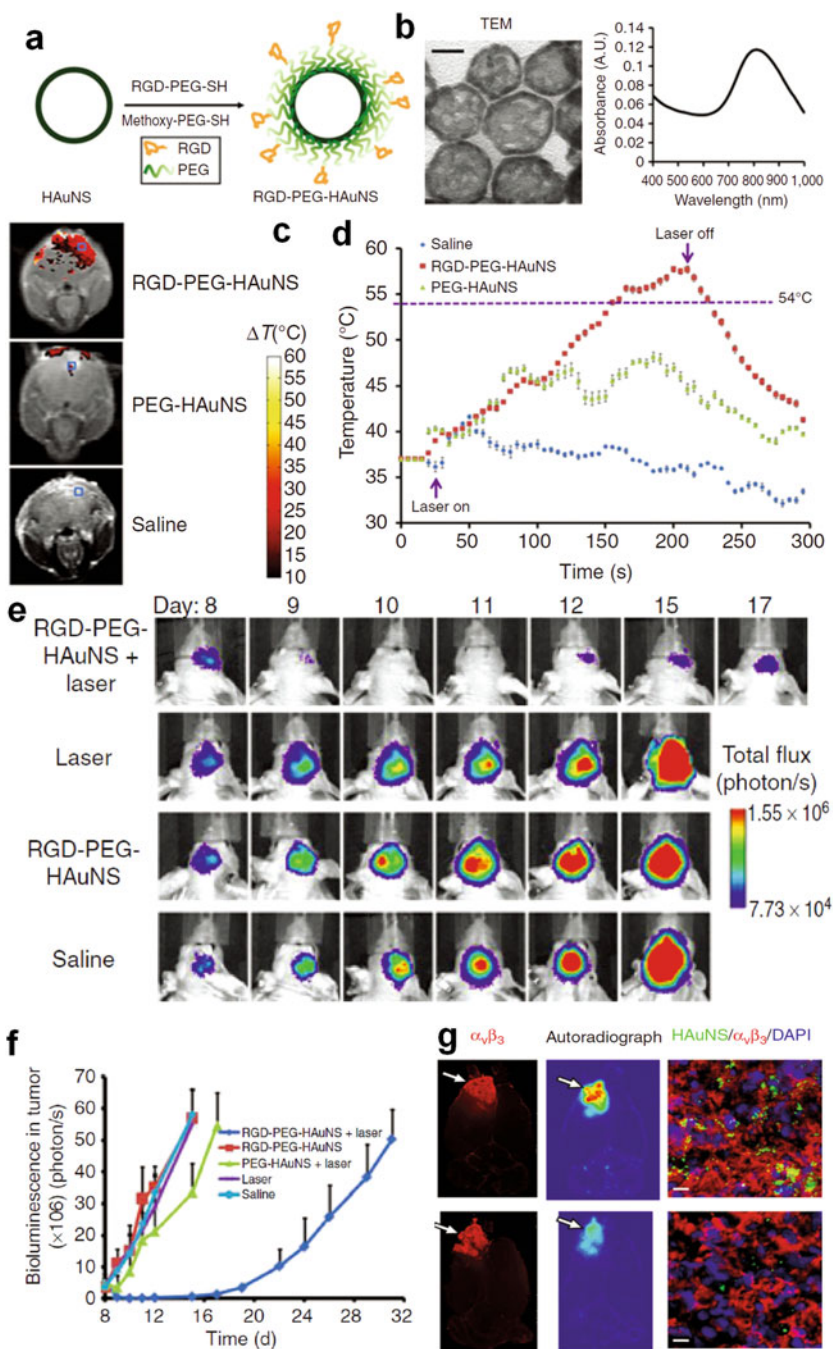
Fig. 1.9 (**a**) Scheme for c(KRGDf)-PEG-modified hollow AuNS (HAuNS). (**b**) TEM image and UV-visible spectrum of the nanoparticles. (**c**) Overlap of mouse brain T1-weighted magnetic resonance imaging (MRI) and MR temperature imaging at the end of laser irradiation. (**d**) Plots of tumor temperature change versus time in the region of interest (*blue rectangles in c*) during a laser (16 W/cm^2 at 808 nm) irradiation. (**e**, **f**) After different treatments, the bioluminescence images

imaging and cancer photothermal ablation. Ke et al. developed AuNSs microcapsule-based ultrasound contrast agents as a multifunctional theranostic agent for imaging-guided photothermal therapy. HeLa cells incubated with AuNSs microcapsules in vitro could be killed photothermally by exposure to NIR light, and the microcapsules maintained adequate acoustic properties that are required to act as an ultrasound contrast agent. The dual-functional theranostic composite holds great potential for ultrasound-guided photothermal cancer therapy [138]. Recently, Ma et al. constructed a multifunctional drug delivery platform based on cholesteryl succinyl silane (CSS) nanomicelles loaded with DOX, Fe_3O_4 magnetic nanoparticles and AuNSs (CDF-AuNSs nanomicelles) to combine MRI, magnetic-targeted drug delivery, light-triggered drug release, and photothermal therapy [139]. An enhancement for T2-weighted MRI is observed for the CDF-AuNSs nanomicelles. These nanomicelles exhibited LSPR absorbance in the NIR region, and a NIR light-triggered DOX release was realized. A synergistic effect of the photothermal therapy and the magnetic-field-guided drug delivery was observed in the presence of both NIR irradiation and magnetic field.

AuNSs provide great advantages for targeted cancer photothermal therapy for the light excitation-guided local heating. However, these nanoshells typically synthesized between 80 and 150 nm in diameter may be restricted for medical application for the quick clearance by the reticulum endothelial system (RES) and a limited diffusion within tissue. Therefore, it's necessary to overcome the challenge in the size of AuNSs and facilitate their biomedical applications [140].

1.6 Au Nanorods (AuNRs)

AuNRs are another kind of Au nanostructures which have been extensively investigated for cancer theranostics in the past few years. Due to their anisotropic shapes, AuNRs exhibit two LSPR absorbance peaks: the transverse mode at ~515 nm and the longitudinal mode whose position depends on the aspect ratio of the rod and can be finely tuned from visible to NIR region. AuNRs have been proved to be promising in a wide range of biomedical applications such as imaging, hyperthermia therapy, and drug delivery due to their unique LSPR and photothermal effects. Recently, AuNRs have been explored to combine imaging diagnosis and therapeutic treatment to function as NIR light-triggered theranostic platform.

Fig. 1.9 (continued) (**e**) and quantitative analysis (**f**) of nude mice bearing the luciferase gene-transfected U87-TGL human glioma tumors on day 8 after tumor inoculation. (**g**) Targeted delivery of ^{64}Cu-labeled c (KRGDf)-PEG-HAuNS to U87 cells in mouse brain. The *left* shows the photographs of mouse brains stained with hematoxylin and eosin (H&E) and $\alpha_v\beta_3$; the *middle* shows the location of HAuNS according to autoradiographs of mouse brains; the *right* shows immunofluorescence micrographs of tumor tissue at high magnification. The *red color* indicates the integrin $\alpha_v\beta_3$; the *green* indicates scattering signal of HAuNS under dark field; the *blue* indicates 40,6-diamidino-2-phenylindole (DAPI)-stained cell nuclei; the *arrows* indicate tumors with the bar of 10 μm (Reprinted with permission from ref. [129]. Copyright 2011, American Association for Cancer Research)

AuNRs were first reported as reagents for simultaneous molecular imaging and photothermal cancer therapy by El-Sayed et al. in 2006 [44]. They conjugated AuNRs with anti-EGFR antibodies and applied them to target and treat malignant oral epithelial cell lines. Using dark-field imaging and photothermal therapy, the malignant cells could be diagnosed and destroyed simultaneously. Due to the selective targeting, malignant cells required only half the laser energy to be photothermally destroyed than the nonmalignant cells. Later, imaging-guided hyperthermia therapy became the most investigated combination theranostic strategy. Many researchers reported the AuNRs-mediated cancer imaging and photothermal therapy, and targeting molecules are often conjugated to AuNRs for active targeting. For instance, Huff et al. found that both CTAB-AuNRs- and folate-AuNRs-mediated heating could produce severe blebbing in cell membranes and render them permeable to chemical regents. The former was found to be internalized into KB cells within hours, while the latter was accumulated on the cell surface over the same time interval [141]. Black et al. conjugated AuNRs with deltorphin, a high-affinity ligand for delta opioid receptor (δOR) which expressed on human colon carcinoma HCT-116 cell line. Selective imaging and photothermal ablation were observed in receptor-expressing cells while not in cells that did not express the receptor in a mixed population of cells [119]. By conjugation AuNRs with a NIR fluorescent dye through a peptide linker, which could be degraded by matrix metalloprotease (MMP), Yi et al. demonstrated the quenching effect of AuNRs and the recovery of quenched fluorescence when the substrate was degraded by MMP enzymes secreted by cancer cells [142]. The expression of MMP and cancer progress imaged by the recovery of quenched fluorescence and photothermal cancer therapy were realized simultaneously. Choi et al. attached epithelial cancer cells targeting molecules cetuximab (CET) to PEG-AuNRs (CET-AuNRs) and assessed their targeting, imaging, and photothermal therapy behavior [143]. In vivo NIR absorption imaging revealed that CET-AuNRs accumulated in the tumor region after intravenously injection, while CET-free AuNRs did not. Histological analysis of excised tumor tissue showed that CET-AuNRs-treated tumors exhibited severe cellular damage compared to the nontreated control after NIR laser irradiation.

Recently, imaging-guided dual modal cancer treatment has been developed to improve the therapy efficacy. For instance, Kuo et al. designed a fluorescent AuNRs conjugate to simultaneously serve as photodynamic therapy (PDT) and hyperthermia agents [144]. The conjugate was prepared by coating AuNRs with poly (styrene-alt-maleic acid) (PSMA) and ICG, a hydrophilic and anionic photosensitizer in sequence via electrostatic interaction. This theranostic nanoplatform combining fluorescence imaging of ICG, PDT, and hyperthermia could more efficiently extinguish cancer cells than PDT or hyperthermia treatment alone. Jang et al. constructed an AuNR-photosensitizer complex for noninvasive NIR fluorescence imaging and combined PDT and photothermal cancer therapy [145]. Fluorescence emission and singlet oxygen generation by photosensitizer AlPcS4 were quenched after conjugation with AuNRs. Increased cellular uptake and in vitro phototoxicity were observed in AuNR-AlPcS4-treated cells than in free AlPcS4-treated cells. In vivo, efficient NIR fluorescence imaging of tumor sites and improved therapeutic efficacy were

obtained by PDT and photothermal dual therapy. Huang et al. developed folic acid-conjugated silica-modified AuNRs for simultaneously targeting, X-ray/CT imaging, radiotherapy, and photothermal therapy [73]. The multifunctional theranostic nanoplatform exhibited excellent imaging and targeting ability for X-ray/CT imaging-guided dual-mode enhanced radio- and photothermal therapy. Recently, Zhang et al. have designed a triple-modal functional AuNRs for in vivo fluorescence imaging, SERS detection, and photodynamic therapy [146]. SERS and fluorescence agents are chemically doped in different layers of a silica-/polymer-coated AuNR, thereby forming two individual imaging "channels." These nanoparticles could accumulate inside the tumors by intravenously injection, thus allowing detection of the tumor by SERS and fluorescence measurements. Through the same doping method, a PDT photosensitizer, protoporphyrin IX (PpIX), was loaded into the multilayered shell, and PDT treatment could be conducted right after the detection of the tumor.

By using various surface modification or functionalization methods, AuNRs have been developed as NIR light-responsive drug delivery system. Combining photothermal therapy and drug delivery of AuNRs, thermo-chemotherapy was realized for dual treatment of cancer [147, 148]. Our group has designed mesoporous silica-coated AuNRs (Au@SiO$_2$) loaded with DOX for cancer theranostics [95]. Based on the simultaneous imaging, photothermal therapy, and drug delivery property of Au@SiO$_2$, we further developed a thermoresponsive nanocomposite by coating Au@SiO$_2$ with a thermo- and pH-responsive polymer shell, poly(N-isopropylacrylamide-co-acrylic acid), and explored them in vivo applications [109] (Fig. 1.10). The thermoresponsive polymer shell prolonged the blood circulation time of AuNRs, and both local water bath heating and NIR laser irradiation at the tumor site following intravenous administration could increase the nanocomposite accumulation in tumor. The nanocomposite served as targeted cancer thermo-chemotherapy platform which simultaneously delivers heat and anticancer drugs in a NIR laser-activation mechanism. There are also other reports on the application of AuNRs for NIR light-triggered thermo-chemotherapy and imaging. Guo et al. fabricated a chitosan/AuNR (CS-AuNR) hybrid nanosphere for the delivery of the anticancer drug cisplatin [149]. This hybrid nanosphere could serve as multifunctional theranostic platform for simultaneous dark-field imaging and NIR light-mediated thermo-chemotherapy. Xiao et al. conjugated AuNRs with DOX, cRGD, and ^{64}Cu-chelator for combined anticancer drug delivery, targeting, and PET imaging [118]. cRGD-conjugated nanocarriers exhibited improved cellular uptake and cytotoxicity compared to nontargeted ones in vitro.

1.7 Hollow Au Nanospheres (HAuNSs)

HAuNSs are novel Au nanostructures consisting of only a thin Au shell with a hollow interior. Different from solid Au nanoparticles, HAuNSs have LSPR absorption in the NIR region and display strong photothermal conducting properties.
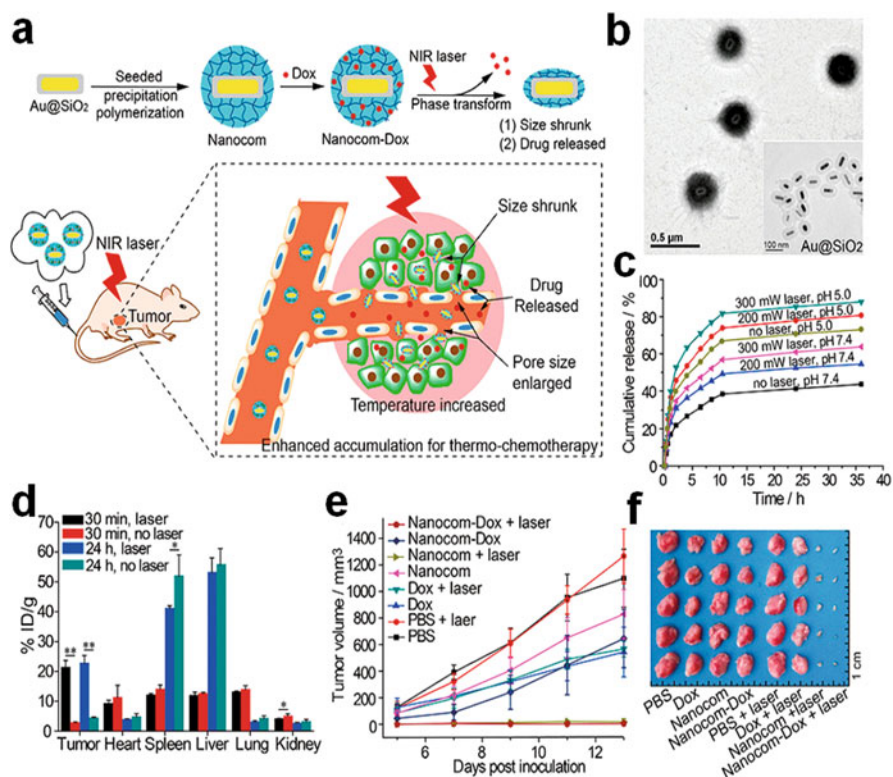
Fig. 1.10 (**a**) Nanocomposite formulation process and NIR laser-induced targeted thermo-chemotherapy using the nanocomposite. (**b**) TEM images of the nanocomposite and Au@SiO$_2$ (*inset*). (**c**) DOX release profiles from Nanocom-Dox with or without NIR laser irradiation at different pHs. (**d**) The biodistribution of the nanocomposite at 30 min and 24 h after systemic administration and NIR laser irradiation at the tumor based on ICP-MS analysis (data expressed as percentage of the injected dose per gram of tissue (% ID/g). *P<0.05 or **P<0.01, significant difference between irradiated and unirradiated groups. (**e**) The antitumor activity including PBS, DOX, Nanocom, and Nanocom-DOX groups (with or without laser irradiation) through tail vein by measuring the tumor volume. (**f**) Tumor dissection photographs through systematic administration (Reprinted with permission from ref. [109]. Copyright 2014, American Chemical Society)

Additionally, HAuNSs can act as drug delivery system due to their hollow interior. Combined with the strong and tunable absorption band in the NIR region, HAuNSs are ideal theranostic platform for simultaneous cancer imaging and thermo-chemotherapy. Additionally, the size of HAuNSs (30–50 nm in diameter) is much smaller than AuNSs (>120 nm) and therefore exhibits increased extravasation from tumor blood vessels and higher intracellular uptake by mammalian cells.

To achieve targeted delivery, Melancon et al. covalently conjugated HAuNSs with C225, a monoclonal antibody to EGFR (C225-HAuNSs). By using scattered imaging from the nanoshells, EGFR-mediated selective uptake of C225-HAuNSs but not IgG-HAuNS control in EGFR-positive A431 tumor cells was observed. Irradiation of A431 cells treated with C225-HAuNSs with NIR laser resulted in

selective destruction of these cells. The cells treated with C225-HAuNS alone, laser alone, or IgG-HAuNS plus NIR laser were not affected on cell viability [150]. Lu et al. conjugated HAuNSs with α-melanocyte-stimulating hormone (MSH) analog, [Nle[4], D-Phe[7]]α-MSH (NDP-MSH), to develop melanoma-targeted HAuNSs, NDP-MSH-PEG-HAuNSs [151]. Enhanced extravasation and distribution of NDP-MSH-PEG-HAuNSs into tumor matrix were observed compared to nontargeting HAuNS. Furthermore, selective photothermal ablation of B16/F10 melanoma with NDP-MSH-PEG-HAuNSs was confirmed by histological and [^{18}F] fluorodeoxyglucose positron emission tomography evaluation at 24 h post NIR laser irradiation. The same group also reported gene delivery by targeted HAuNSs-mediated photothermal transfection [152]. NF-κB downregulation was achieved by NIR light and folate receptor-targeted HAuNSs carrying siRNA, recognizing NF-κB p65 subunit. Using micro-PET/CT imaging, the targeted HAuNSs exhibited higher tumor uptake in nude mice bearing HeLa cervical cancer xenografts than nontargeted nanoparticles. Downregulation of NF-κB p65 was observed only in tumors irradiated with NIR light but not in nonirradiated tumors grown in the same mice, which indicated the gene silence was mediated by controllable cytoplasmic delivery of siRNA through photothermal effect. Combined treatments with p65 siRNA photothermal transfection and chemotherapeutic agent irinotecan caused substantially enhanced tumor apoptosis and growth delay compared to other treatment regimens, which indicated photothermal transfection of NF-κB p65 siRNA could enhance sensitivity to chemotherapeutic agents. Lu et al. also reported theranostic HAuNSs with multi-functions including tumor targeting, PAT imaging, and photothermal therapy [129]. By targeting brain tumor receptors via RGD peptides, the theranostic HAuNSs exhibited highly specific tumor diagnosis. Combined with the photothermal therapy, a decrease in tumor volume for up to 3-week post NIR laser treatment was observed in an orthotopic mouse xenograft model of glioma by targeting brain tumor receptors.

Li's group also did a series of excellent works on HAuNSs-mediated cancer theranostics [153–156]. They reported exceptionally high payload of DOX in HAuNSs for NIR light-triggered drug release, photothermal therapy, as well as dark-field imaging in vitro. As high as 63 % DOX by weight could be loaded to PEG-coated HAuNS since DOX was coated to both the outer and the inner surfaces of HAuNSs. Combined thermo-chemotherapy exhibited significantly greater cell killing when MDA-MB-231 cells were treated with DOX-loaded HAuNSs plus NIR light [154]. In another work, the thermo-chemotherapy efficacy of DOX-loaded PEG-coated HAuNSs with DOX:PEG:HAuNS weight ratio of 1:3:1 (NP3) was studied in vitro and in vivo using human MDA-MB-231 breast cancer and A2780 ovarian cancer cells [156]. In vitro, significantly greater cell killing was observed when cells were treated with both NP3 and NIR light irradiation, which is attributable to the combined photothermal therapy and the released DOX. In vivo, NP3 exhibited slower clearance in blood and greater accumulation in tumors than free DOX, which was demonstrated by μPET images of mice bearing A2780 tumors after intravenous injection of ^{64}Cu-labeled NP3. NP3-mediated thermo-chemotherapy demonstrated greater antitumor activity than free DOX, NP3, or liposomal DOX, which represents a promising approach to effective anticancer therapy. DOX-loaded

HAuNSs can be further conjugated with a cyclic peptide targeting EphB4, a member of the Eph family of receptor tyrosine kinases that are overexpressed on the cell membrane of multiple tumors and angiogenic blood vessels.

Li et al. also observed an increased uptake of targeted nanoparticles (T-DOX@ HAuNSs) in three EphB4-positive tumors both in vitro and in vivo [155]. By dual-radiotracer technique, in vivo release of DOX from DOX@HAuNS triggered by NIR laser was confirmed. Enhanced antitumor effect was obtained when mice were treated with T-DOX@HAuNSs plus NIR laser irradiation compared to nontargeted DOX@HAuNSs plus laser or HAuNSs plus laser. These results demonstrated that NIR light-guided thermo-chemotherapy with a single nanoplatform is capable of mediating simultaneous imaging, photothermal therapy, and local drug release which has great promise as a new cancer theranostic regime.

The authors also investigated the impact of nanoparticle-mediated localized hyperthermia on vascular permeability to enhance the efficacy of chemotherapy. By conjugating an anti-EGFR monoclonal antibody C225 to HAuNSs (C225-HAuNSs), they studied the vascular permeability and subsequent uptake of a water-soluble polymer using a combined approach with magnetic resonance temperature imaging (MRTI), ultrasound, and optical imaging [157]. MTRI showed a maximum temperature of 65.2 ± 0.10 °C and 47.0 ± 0.33 °C in A431 tumor xenograft of mice treated with C225-HAuNSs plus laser and saline plus laser, respectively. Dynamic contrast-enhanced magnetic resonance imaging (DCE MRI) demonstrated greater than twofold increase of DTPA-Gd in the initial area in mice injected with C225-HAuNS and exposed to NIR laser compared with control mice. Increased vascular perfusion was confirmed by Power Doppler ultrasound, which revealed a four- to sixfold increase in percentage vascularization in mice treated with C225-HAuNSs plus NIR laser compared to control mice. Based on NIR fluorescence imaging, intratumor accumulation of a model polymeric drug PG-Gd-NIR813 5 min post-laser therapy was significantly higher than those at 24 h-post laser therapy and the saline-treated ones. These results suggested photothermal effect of C255-HAuNSs in tumor site could increase the vascular perfusion and therefore enhance the permeability of chemotherapeutic agents to the tumors.

1.8 Au Nanocages (AuNCs)

AuNCs represent a novel class of Au nanostructures firstly synthesized by Xia's group in 2002 [158]. The LSPR peak position of the AuNCs is tunable from the visible to the NIR region, which makes them attractive for colorimetric sensing and biomedical applications. The extraordinarily large scattering and absorption cross sections of AuNCs endow them superb optical tracers or contrast agents for various imaging modalities such as dark-field microscopy, optical coherence tomography, photoacoustic tomography, and multiphoton luminescence imaging. Additionally, the hollow interiors of AuNCs can be used for drug encapsulation, and the porous walls can facilitate the drug release controlled by various stimuli such as hyperthermia. During the past decades, researchers have extensively explored the

applications of AuNCs in a variety of biomedical applications ranging from sensing to imaging, diagnosis, and cancer theranostics.

AuNCs have been conjugated with various ligands for selective tumor targeting and imaging. Xia et al. have quantitatively investigated the passive targeting of PEG-functionalized AuNCs in a tumor mouse model [159]. The amount of AuNCs distributed in tumor reached 3.4 ± 0.9 %ID/g at 24 h postinjection, while the distributions of AuNCs in normal tissues were low. The same group also compared the passive and active targeting efficiencies of AuNCs for melanomas based on in vivo photoacoustic imaging [66]. AuNCs were conjugated with [Nle^4,D-Phe^7] α-melanocyte-stimulating hormone (NDP-MSH), a peptide which selectively binds to the α-MSH receptors overexpressed on melanoma. The photoacoustic signal in the melanoma was much stronger for the NDP-MSH-conjugated AuNCs than that of nontargeted AuNCs, which demonstrated an enhanced uptake of AuNCs by the tumor due to active targeting.

The initial study on the ability to destroy cancer cells in vitro by AuNCs-mediated photothermal effect was also demonstrated by Xia's group [160, 161]. They also studied the efficacy of photothermal cancer treatment in a tumor mouse model in vivo [162]. PEGylated AuNCs were administrated intravenously to tumor-bearing mice, and the tumor on the right flank of each mouse was irradiated with NIR laser. The tumors treated with AuNCs were rapidly heated to temperatures over 55 °C, while no change was observed for the control. [^{18}F] fluorodeoxyglucose (^{18}F-FDG) positron emission tomography was applied to evaluate the response to the photothermal therapy. The normalized values suggest a decrease in metabolic activity by 70 % after AuNCs plus laser treatment compared to the untreated mice.

AuNCs have also been developed as drug delivery systems for cancer theranostics by integrating optical imaging and thermo-chemotherapy. Yavuz et al. coated the surface of AuNCs with a smart polymer, poly(N-isopropylacrylamide) (pNIPAAm) and its derivatives, which can change conformation in response to temperature variation at a point known as the low critical solution temperature (LCST) [163]. Under NIR laser irradiation, the temperature will increase due to the photothermal effect of AuNCs. The polymer chains collapse as the temperature increases beyond the LCST, which expose the pores of the nanocages and allow thus the preloaded drugs to be released. Moon et al. reported an AuNCs-based theranostic system, combining photoacoustic imaging and controlled drug by high-intensity-focused ultrasound (HIFU) [164]. The system was fabricated by filling the hollow interiors of AuNCs with a phase-change material (PCM) such as 1-tetradecanol that has a melting point of 38–39 °C. The PCM-loaded AuNCs simultaneously enhanced photoacoustic imaging contrast and demonstrated highly effective drug release ability triggered by HIFU or heat. PCM can reversibly change its physical state between solid and liquid according to the local temperature. When exposed to direct heating or HIFU, the PCM will melt and escape from the interiors of AuNCs through small pores on the surface, which allow the concurrent release of the encapsulated drugs. Since HIFU is a deeply penetrating energy source, the drug release profile could be controlled by adjusting the power of HIFU and/or the duration of exposure to HIFU. Shi et al. demonstrated the application of AuNCs in thermo-chemotherapy based on calcium phosphate-coated magnetic nanoparticles (Fe$_3$O$_4$@CaP)-capped

AuNCs [165]. This nanoplatform integrated magnetic targeting, photothermal therapy, and chemotherapy for killing cancer cells. The cell killing efficacy of DOX-loaded AuNCs under NIR irradiation was higher than the sum of chemotherapy of DOX-loaded AuNCs and AuNCs-induced photothermal therapy, which indicated the combined cancer thermo-chemotherapy resulted in a synergistic effect. Additionally, the magnetic component in the nanoplatform could potentially be used as an MRI contrast agent and targeted drug delivery.

1.9   Au Nanostars

Au nanostars contain multiple sharp branches with plasmons tunable in the NIR region, which have gained wide interest in biomedical areas including SERS spectroscopy, photoacoustic imaging, biosensing, photodynamic, and photothermal therapy. The extinction spectra of individual Au nanostars revealed that these nanoparticles have multiple plasmon resonances varying greatly due to shape polydispersity. Therefore, Au nanostar exhibits broad absorption peaks due to overlapping of many distinct spectra.

Yuan et al. functionalized Au nanostars with TAT-peptide, a cell-penetrating peptide encoded by human immunodeficiency virus type 1 (HIV-1), in order to increase the intracellular delivery of Au nanostars [166]. TAT-peptide-functionalized nanostars were found to enter cells more frequently than bare or PEGylated nanostars. The enhanced intracellular delivery in turn allows efficient photothermal therapy with lower irradiance. After incubation of TAT-nanostars on BT549 breast cancer cells, photothermal ablation was accomplished ultralow irradiance (0.2 W/cm^2), which is the lowest value ever reported for pulsed laser-induced photothermal therapy and below the maximal permissible exposure of skin. Both TPL and TEM imaging confirmed that the uptake mechanism of TAT-nanostars primarily relies on actin-driven lipid raft-mediated macropinocytosis. The same group also demonstrated the use of Au nanostars for particle tracking via TPL imaging and simultaneous Au photothermal therapy [167]. They demonstrated photothermal ablation of SKBR3 breast cancer cells incubated with bare nanostars within 5 min of irradiation in vitro. In vivo, PEGylated nanostars were injected intravenously into a mouse for 2 days, then extravasation of nanostars was observed, and localized photothermal ablation was demonstrated on a dorsal window chamber. Au nanostars interact intensely with incident light enabling highly sensitive in vivo tracking in the vasculature. Combined hyperthermia and photodynamic therapy (PDT) and upon single continuous wave (CW) laser using photosensitizer-functionalized Au nanostars were reported (Fig. 1.11) [168]. Chlorine 6 (Ce6), a commonly used photosensitizer,

Fig. 1.11 (continued) at 4 h postinjection of PBS, Ce6, GNS-PEG, and GNS-PEG-Ce6. (**f**) Tumor volume after laser irradiation treatment over time. (**g**) The ultrasound (*upper row*) and photoacoustic (*lower row*) imaging of tumor-bearing mice after laser irradiation with the same procedure as above. The *circles* indicate the region of interest in the tumors, and the *blue* shows the hypoxia state in the tumors. *Scale bars*: 1 mm (Reprinted with permission from ref. [168]. Copyright 2013, John Wiley & Sons, Inc.)
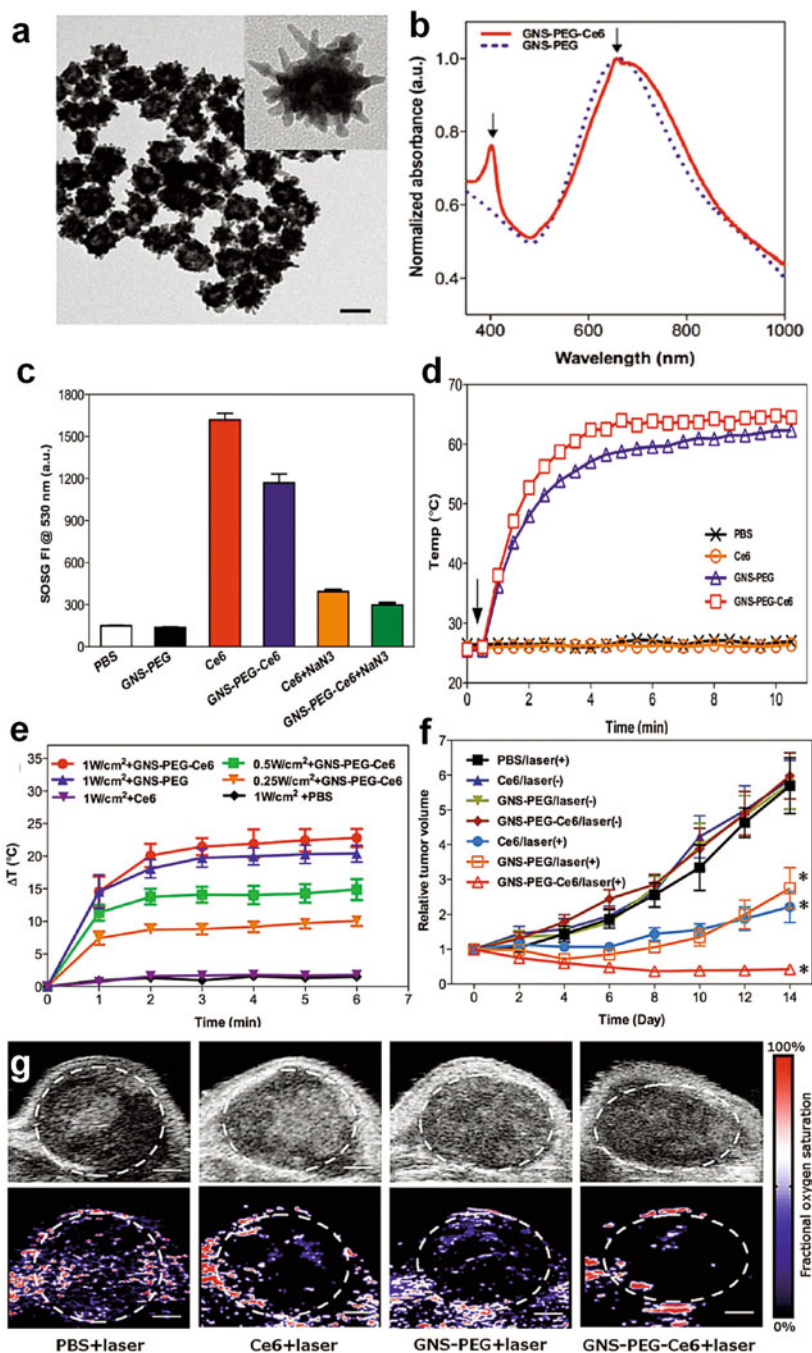
Fig. 1.11 (**a**) TEM images of Au nanostars (GNSs). (**b**) UV-vis-NIR spectra of GNSs. (**c**) The generation of free radicals under irradiation determined by the SOSG fluorescence intensity. (**d, e**) Temperature curves of different GNSs (**d**) and GNS-treated tumors (**e**) irradiated by laser over time. The MDA-MB-435 tumor-bearing mice are exposed to 671 nm laser (1.0 W/cm²) for 6 min

was covalently anchored on the surface of Au nanostars. To induce both hyperthermia and PDT effect by a single NIR CW laser, they adapted the LSPR of Au nanostars to fit that of Ce6. This strategy significantly improved the anticancer effect and simplified the treatment process. These results suggested Au nanostars as promising theranostic agents for cancer therapy.

1.10   Other Au Nanostructures

Other Au nanostructures including nanoroses, nanobubbles, and nanoparticles have also been investigated for their application in cancer theranostics. Lapotko et al. first reported laser-activated micro- and nanobubbles that were produced around plasmonic nanoparticles in cells [169]. These intracellular bubbles were found to be the universal phenomena that can be used for sensitive and noninvasive monitoring of individual cell. Systematic researches have been done to investigate the properties and biomedical applications of Au nanobubbles such as thermolysis of cancer cells, cell imaging, gene, and drug delivery [170–174]. Wagner et al. developed plasmonic nanobubbles (PNBs) as an in vivo tunable theranostic cellular agent in zebrafish hosting prostate cancer xenografts [170]. Plasmonic nanobubbles were selectively generated around Au nanoparticles in cancer cells in the zebrafish with short single-laser pulses. Two different-sized PNBs were produced by varying the energy of the laser pulse: an initial small PNB for detecting cancer cells by optical scattering, followed by a second bigger PNB for mechanically ablating cells. These results demonstrated that PNBs could be applied for the diagnosis and guided ablation of individual cancer cells in a living organism without damage to the host.

Recently, Hu et al. has reported a novel theranostic system based on Au cubic nano-aggregates as potential photoacoustic contrast and photothermal therapy [175]. The cubic Au nano-aggregates structure with edge-length of 80 nm (Au-80 CNAs) was synthesized with a simple and cost-effective method and exhibited strong NIR absorption, excellent water-solubility, and good photothermal stability. The temperature of the solution containing Au-80 CNAs (100 μg/mL) increased by about 38 °C under 808 nm laser irradiation for 5 min. Both in vitro and in vivo studies demonstrated that Au-80 CNAs were potent photothermal therapeutic agents and photoacoustic imaging contrast agents. Ma et al. reported a nanocluster of Au-coated iron oxide primary particles (nanoroses) for targeted cellular imaging and therapy [176]. The stable uniformly sized (ca. 30 nm) nanoclusters were NIR active, superparamagnetic formed by kinetically controlled self-assembly of Au-coated iron oxide nanoparticles. The nanoroses exhibited an order of magnitude larger than observed for typical iron oxide particles with thicker Au shells, because of the thin Au shells with an average thickness of only 2 nm. High uptake of the

nanoclusters by macrophages is facilitated by the small size of the nanoclusters and the dextran surface coating, which further provided intense NIR contrast in dark-field and hyperspectral microscopy, both in vitro and in vivo.

Solid Au nanoparticles (AuNPs) have been demonstrated as a novel CT contrast agent in blood pool imaging (angiography) and for diagnosis of hepatoma in vivo. Kim et al. reported multifunctional AuNPs for targeted molecular CT imaging and therapy of prostate cancer [177]. By functionalizing the surface of AuNPs with a prostate-specific membrane antigen (PSMA) RNA aptamer that binds to PSMA, they established a targeted CT imaging system for specifically imaging of prostate cancer cells that overexpressed the PSMA protein. Besides, the PSMA-specific aptamer formed a GC-rich duplex that acts as a loading site for the chemotherapeutic agent DOX, which enables combined prostate cancer imaging by CT and anticancer therapy. PSMA aptamer-conjugated AuNPs exhibited more than fourfold greater CT intensity for targeted LNCaP cells than that of nontargeted cells. Furthermore, DOX-loaded aptamer-conjugated AuNPs were more potent to kill targeted cancer cells than nontargeted cells, suggesting target-specific drug delivery [178].

A novel kind of nanoparticles has been explored by replacing the silica cores in traditional nanoshells with an Au-sulfide core structure. Zhou et al. first synthesized Au-Au sulfide nanoparticles (GGS NPs) that exhibited strong NIR-absorbing properties [179]. GGS NPs with a LSPR between 800 and 900 nm for therapeutic and imaging applications are generally synthesized in the range of 35–55 nm in diameter, much smaller than Au silica nanoshells which range from 120 to 140 nm for the same resonant wavelength [180]. Models have suggested that particles with diameter <100 nm could improve tumor extravasation [181], and experimental data also suggested that the greatest uptake of Au occurred in diameters between 30 and 50 nm [182]. Therefore, GGS NPs may prove advantageous in cancer therapeutic and imaging. Day et al. developed NIR-resonant GGS NPs as dual contrast and therapeutic agents for cancer theranostics [183]. After conjugation with anti-HER2 antibodies, GGS NPs could specifically bind SK-BR-3 breast carcinoma cells that overexpressed the HER2 receptor. TPL imaging of the cancer cells was obtained with irradiation by low energy pulsed-NIR laser (1 mW). Higher laser powers were applied for photothermal ablation of the cancerous cells (50 mW), which resulted in extensive membrane blebbing and cell death.

Gobin et al. investigated in vivo distribution of GGS NPs and found that these NPs remained in circulation longer than Au/silica nanoshells greater than 24 h [184]. Accumulation in the liver, spleen, and tumors showed that larger dose GGS NPs could avoid RES clearance and accumulate in tumors. Photothermal ablation of tumor cells with NIR irradiation of the GGS NPs resulted in increased survival of mice. With further optimization of laser power and NPs functionalization, GGS NPs may be an effective therapeutic agent to compliment the treatment of cancers.

1.11 Strategy for Combatting Cancer Drug Resistance and Inhibiting Cancer Stem Cells and Cancer Metastasis

The photothermal treatment using Au nanostructures can efficiently improve the therapy of cancer cells for drug resistance. Cancer cells develop drug resistance under evolutionary pressure from chemotherapy. They become less sensitive to chemotherapeutic drugs at a low dose compared to the sensitive cancer cells. It still lacks effective and successful approach to overcome drug resistance in clinic. Usually, the resistant cancer cells have little accumulation and low sensitivity of drugs. Wang et al. reported a simple strategy to combat cancer drug resistance using the photothermal properties of mesoporous silica-coated AuNRs. At a mild laser power density, the nanoparticle-mediated hyperthermia doesn't kill resistant cells, but successfully modulate the genes associated to drug resistance. In particular, this photothermal treatment triggers higher expression of heat shock factor (HSF-1) trimers and depresses the expression of P-glycoprotein (Pgp) and mutant p53. As a result, both drug accumulation in the resistant cells and their sensitivity to drugs can be greatly enhanced using NIR laser irradiation [14] (Fig. 1.12). Moreover, laser treatment of AuNRs can not only produce photothermal effects but also generate free radicals such as singlet oxygen [185, 186]. Resistant cells retain a low redox state, and the levels of reactive oxygen species are elevated due to laser irradiation on AuNPs [187]. To combine photothermia, the generation of free radicals, and chemotherapy, AuNR-based platform can successfully combat resistance due to the synergetic roles under laser treatment.

The photothermal treatment using Au nanostructures can also inhibit cancer stem cells (CSCs). These cells are found in a variety of cancers and resistant to chemotherapy and X-ray radiation therapy. Eradication of CSC cell population should provide a choice to cancer therapy. Our group reported that photothermal treatment of AuNRs can eliminate CSCs in breast cancer cells (MCF-7). As shown in Fig. 1.13, photothermal therapy significantly reduces the aldehyde dehydrogenase positive (ALDH$^+$) cells subpopulation and the mammosphere formation ability of treated cells. The treatment also decreases the expression of stem cell markers and inhibits CSCs more significantly compared to non-CSCs because CSCs have a greater cell uptake of AuNRs to generate stronger heat stimulus. Furthermore, salinomycin (SA), a CSCs inhibitor, is loaded with polyelectrolyte-modified AuNRs to combine chemotherapy and thermal therapy. Due to triggered drug release and hyperthermia with laser irradiation, the synergistic effect can efficiently inhibit CSCs [188].

Our group also reported that CTAB-capped AuNRs with serum protein coating are capable of inhibiting tumor metastasis in vitro and in vivo. The major source of cancer-related deaths is not from the primary tumor itself but from metastasis to
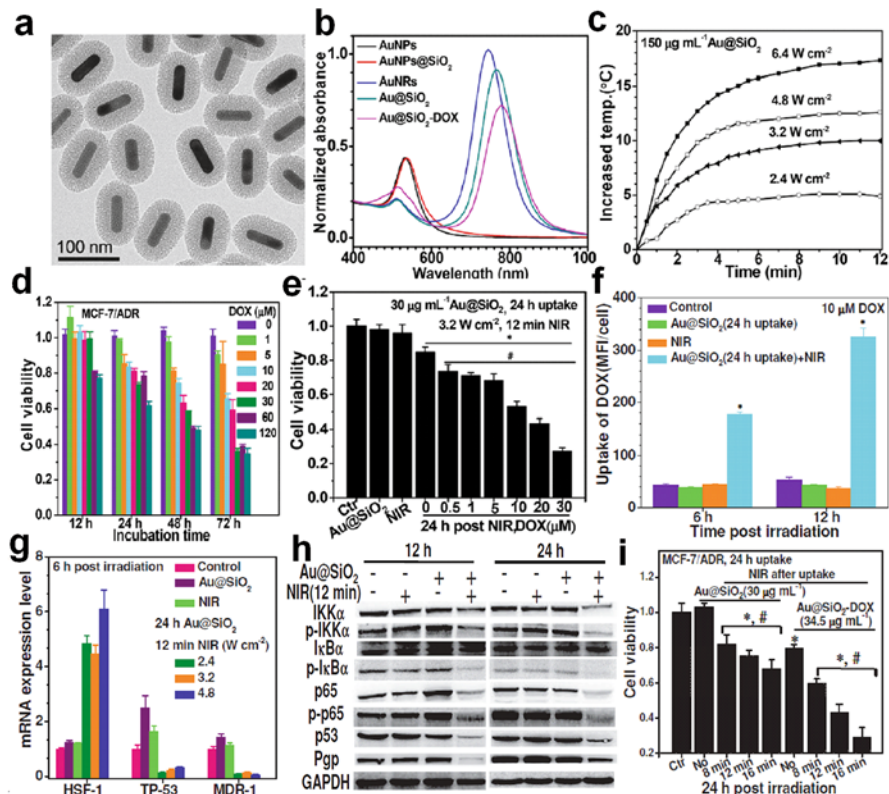
Fig. 1.12 Mesoporous silica-coated AuNRs (Au@SiO$_2$) as a platform to overcome chemotherapeutic resistance with a laser irradiation. (**a**) TEM image of Au@SiO$_2$ nanocarrier. (**b**) Optical absorption properties of AuNRs, Au@SiO$_2$, and DOX-loaded Au@SiO$_2$(Au@SiO$_2$-DOX). (**c**) Temperature curves of Au@SiO$_2$ under 780 nm fs-laser irradiation. (**d**) Dose-dependent cytotoxicity of DOX to the DOX-resistant human breast cancer cell (MCF-7/ADR). (**e**) Photothermal effects of Au@SiO$_2$ on cellular sensitivity to DOX when MCF-7/ADR cells internalize Au@SiO$_2$, and are irradiated by laser, and then are exposed to DOX. (**f**) The influences of laser irradiation on the ability of Au@SiO$_2$-engulfed cells to accumulate DOX. (**g**, **h**) The changes in the expression of resistance-associated genes at mRNA level (**g**) and at protein level (**h**) when MCF-7/ADR cells internalize Au@SiO$_2$ and then are exposed by 780 nm laser irradiation. (**i**) The synergetic effects of photothermia and chemotherapy from Au@SiO$_2$-DOX under laser irradiation to circumvent DOX resistance (Reprinted with permission from ref. [14] Copyright 2014, John Wiley & Sons, Inc.)

other organs in the body. Cancer cells need to invade host tissue, migrate from the primary tumor to blood or lymphatic vessels, translocate to distant sites, extravasate and adapt to new microenvironments, seed there, and form secondary tumors. We reported that serum protein-coated AuNRs exhibit negligible effects on the viability and proliferation metastatic cancer cell lines, but effectively inhibit their migration
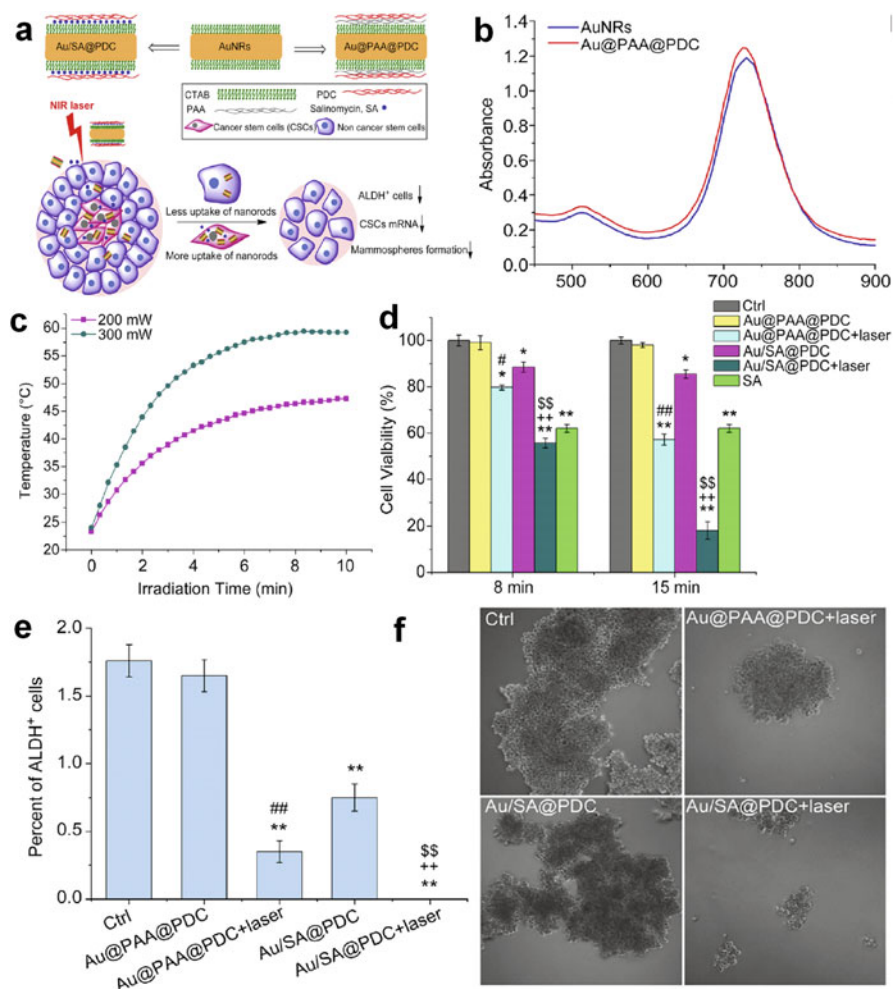
Fig. 1.13 Thermo-chemotherapy strategy to inhibition of breast cancer stem cells (CSCs) using polymer-modified and drug-loaded AuNRs. (**a**) A scheme to demonstrate that AuNRs serve as a combinatorial platform with thermo-chemotherapeutic capability of inhibiting cancer stem cells under laser irradiation. (**b**) UV-vis-NIR spectra of the pristine AuNRs and polyelectrolyte (PAA and PDDAC)-conjugated AuNRs. (**c**) Temperature curves of AuNRs after laser treatment. (**d**) Cell viability of human breast cancer cells (MCF-7) treated with Au@PAA@PDD, Au/SA@PDD, and SA (salinomycin) followed by NIR laser treatment, which triggers hyperthermia and SA release. (**e**) Synergistic inhibition of aldehyde dehydrogenase positive (ALDH$^+$) cells (CSCs) in MCF-7 population by Au/SA@PDC with NIR laser-triggered hyperthermia and SA release. (**f**) Images of mammosphere formation ability of treated cells indicating the characteristic growth and prolifera-tive properties of CSCs (Reprinted with permission from ref. [188]. Copyright 2014, Elsevier, Ltd.)

and invasion in vitro and in vivo (Fig. 1.14). For breast cancer cells (MDA-MB-231) treated with AuNRs or not, both stable isotope labeling by amino acids in cell culture (SILAC)-based proteomics analysis and real-time PCR array have been used to study the protein and mRNA expression. They found that exposure of cells to AuNRs can downregulate the expression of diverse energy generation-related genes, which is due to the inhibitory effects of AuNRs on mitochondrial oxidative phosphorylation (OXPHOS) and glycolysis. The impairment of mitochondrial functions results in a reduction of ATP production and an inhibition of F-actin cytoskeletal assembly, which is crucial for the migration and invasion of cancer cells [189].

1.12   Conclusions and Perspectives

In this chapter, we reviewed the recent progress on NIR light-mediated Au nanostructures for cancer theranostics (Fig. 1.15). During the past decade, Au nanostructures with different geometry and morphology have been synthesized, which possess unique optical and thermophysical properties, enabling multiple imaging and treatment strategies. Great theranostic potential has been revealed for Au nanostructures in serving as imaging contrast agents, photothermal therapy agents, and drug/gene delivery vehicles. More recently, simultaneous realization of imaging, hyperthermia, and chemotherapy in a single theranostic nanoplatform has been developed to optimize the efficacy of cancer treatments. Au nanostructures-mediated cancer theranostics has great advantages including site-specific hyperthermia, NIR light-controllable drug release, and imaging-guided therapy. The multifunctional nanoplatform can generally result in a synergistic effect for optimal treatment efficacy. For the construction of multifunctional theranostic platform, the ease surface modification of Au nanostructures plays a critical role. By noncovalent and covalent functionalization, targeting molecules, imaging contrasts, and chemotherapeutics can be conjugated or encapsulated into a single nanoparticle.

Although a few Au nanostructures have been approved by FDA due to the high biocompatibility, low cytotoxicity, and success in clinical trials [190], there are still challenges in the engineering and in vivo behavior of Au nanostructure-based theranostic platform. The first consideration in the use of Au nanostructures is their toxicity and stability in biological buffers. Au nanostructures are typically synthesized in aqueous media with surface ligands to facilitate their stability. To reduce the toxicity of these non-biocompatible surfactants such as CTAB, native ligands are replaced with neutral polymers, for example, PEG. However, removal of native-stabilizing agent often results in agglomeration of Au nanostructures. Therefore, long-term stability in vivo remains a challenge.

The second challenge is the fundamental understanding of the interaction between Au nanostructures and cells. Recently, our group demonstrated that intracellular localization, not uptake pathway, determines the fate of AuNRs in cancer and normal cells. AuNRs are toxic to cancer cells but not to normal and mesenchymal stem cells. Due to enhanced permeation of the lysosomal membrane of cancer
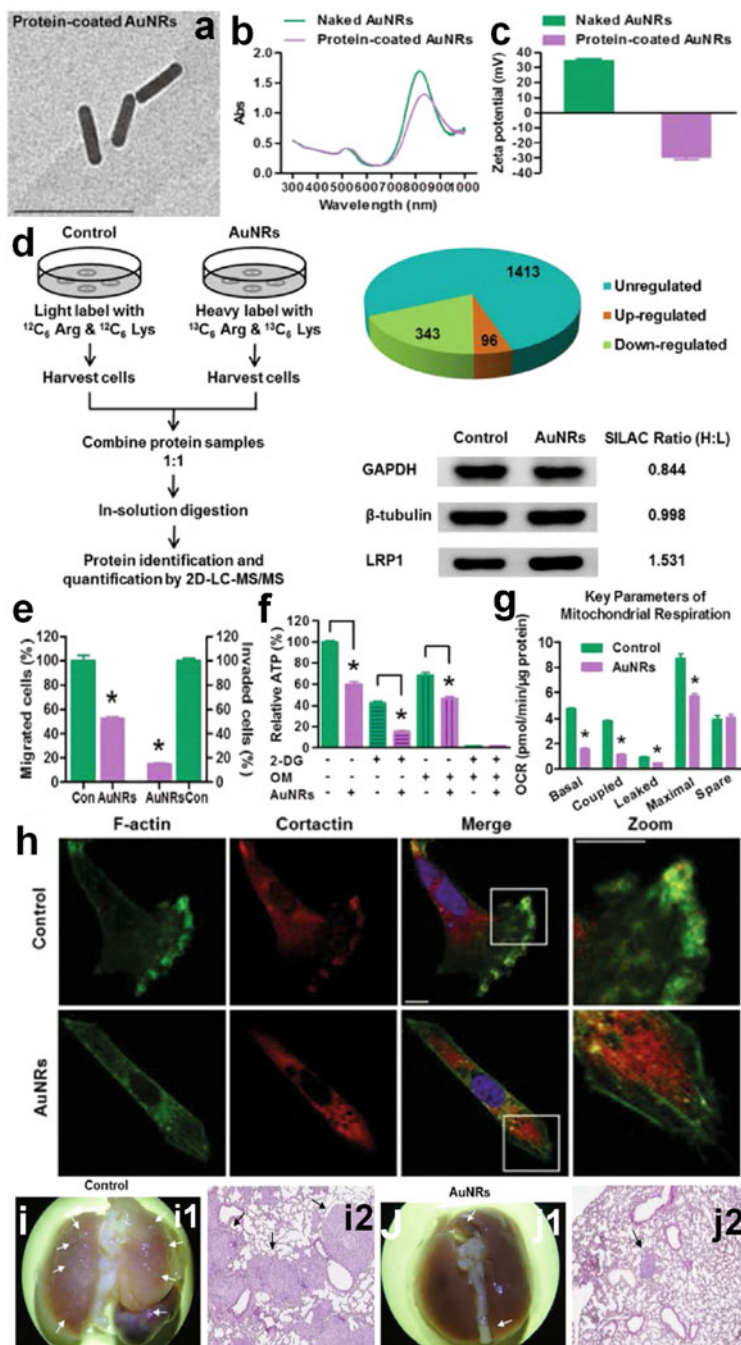
Fig. 1.14 Inhibitory effects of AuNRs on human breast cancer cell migration by disrupting energy metabolism and migration-associated pathway. (**a**) TEM image of protein-coated AuNRs. (**b, c**) UV-vis-NIR spectra and zeta potential of two kinds of AuNRs. (**d**) Stable isotope labeling by amino acids in cell culture (SILAC)-based proteomics analysis of the protein expression related to

cells, nanorods are released into the cytoplasm and transferred from the lysosomes to mitochondria and induce decreased mitochondrial membrane potentials, increasing oxidative stress and finally cell death. However, negligible toxicity was observed in normal cells and mesenchymal stem cells since the lysosomal membrane kept intact. This study provides a detailed understanding of the mechanism of cell-specific cytotoxicity and will guide the design of organelle-targeted Au nanostructures for cancer therapy. The photothermal treatment of Au nanostructures on the cancer-resistant cells and cancer stem cells are also reported, and significant differences exist compared to normal cancer cells [56, 188]. These results suggest the importance of the understanding on the direct interaction between Au nanostructures and different kinds of cells.

The third challenge is to understand the in vivo behavior of Au nanostructure-based theranostic agents including pharmacodynamics, pharmacokinetics, and their toxicity potential in animals and humans. For the past decades, several publications have reported the biodistribution and toxicity of Au nanoparticles [193]. However, systematic studies still lack about how the physicochemical properties of nanoparticles, the types of animals, even their physiological conditions of animals, etc., influence the biodistribution, circulation, translocation, metabolism, degradation, and secretion. Zhang et al. studied the biodistribution of GNRs, Au nanospheres (GNSs) of different sizes, and Au nanoclusters (GNCs) in vivo. They found that the administrated Au nanoparticles into mouse tail vein have a short term of blood circulation (<2 min) and except of hydrolyzed GNCs, most of these nanoparticles distribute in the liver for 28 days. Due to a small size distribution of GNCs, these hydrolyzed GNCs mainly reside in the kidney with high contents even 7 days postinjection. Except of 50 nm GNSs, most nanoparticles can be removed by secreting into urine [194]. For a long-term study, the liver and spleen are the major organs to accumulate these Au nanoparticles, which were consistent with our previous report [195]. Using X-ray absorption spectroscopy, we revealed that AuNRs in the liver and spleen remain stable chemical forms as elemental Au rather than ionic Au that is much toxic than NPs. To study the biocompatibility of Au nanoparticles of a larger size (>20 nm), we can exclude the possible degradation into ions in vivo but consider the effects from the properties such as surface chemistry, shape, size, etc.

Fig. 1.14 (continued) energy generation after MDA-MB-231 cells are treated with AuNRs. The *left* scheme represents SILAC strategy coupled with 2D-LC-MS/MS. The *right* indicates number of modulated proteins by AuNRs and the representative protein quantitative confirmation using western blot analyses. (**e**) The effects of AuNRs on the migration and invasion abilities of cancer cells, using transwell migration and invasion assays. (**f**) Effects of AuNRs on the intracellular ATP level, using a luciferase-based luminescence assay that is normalized to protein concentrations. Before ATP measurement, the cells are pretreated with or without 100 mM 2-deoxyglucose (2-DG), 1 μM oligomycin (OM), or 50 μ M AuNRs for 24 h. (**g**) Effects of AuNRs on the oxygen consumption rate (OCR) in the presence or absence of AuNRs that is monitored using the Seahorse XF24 Extracellular Flux Analyzer in real time. (**h**) Impairment of F-actin cytoskeletal assembly by AuNRs in cancer cells. (**i**) The bright images (*i1*) and the section images (*i2*) after H&E staining for metastatic nodules of tumor on the lung surface of mice. (**j**) The corresponding images of metastatic nodules of tumor after the mice are administered by tail-vein injection with AuNRs (Reprinted with permission from ref. [189]. Copyright 2014, John Wiley & Sons, Inc.)
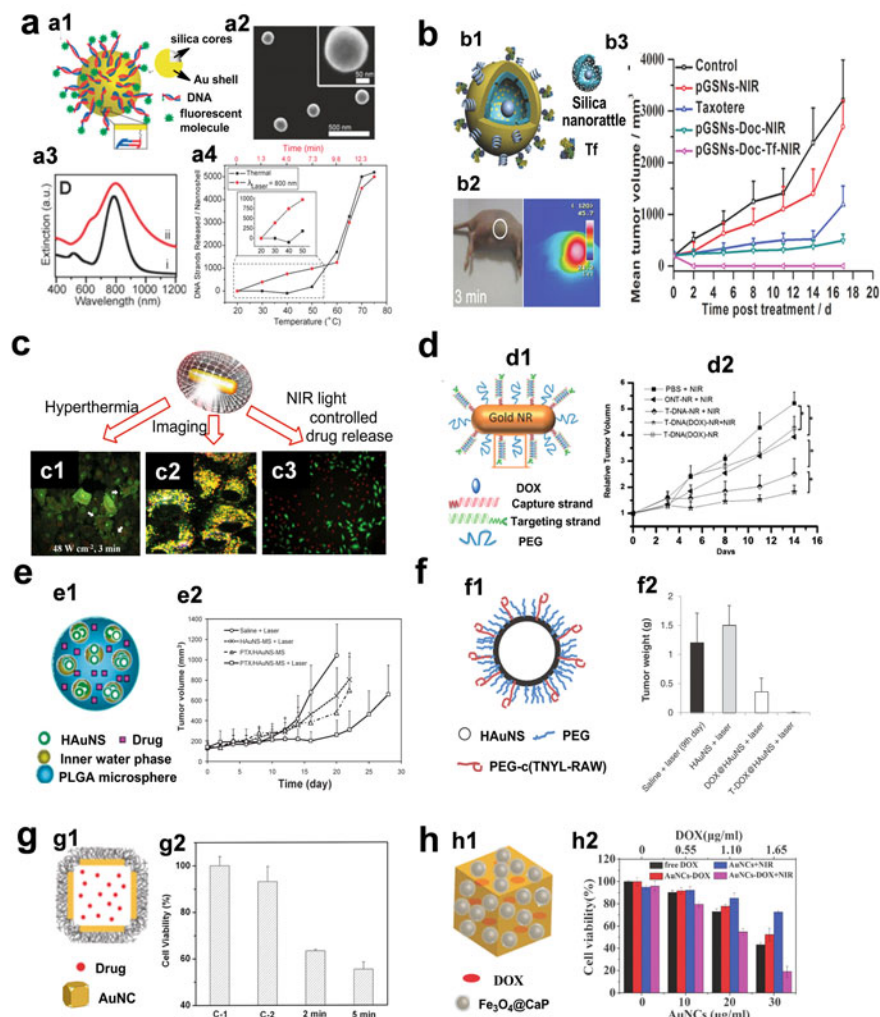
Fig. 1.15 Brief summary for applications of Au nanostructures as NIR light-mediated platforms for cancer theranostics. (**a**) Thermal- and light-triggered release of ssDNA from Au nanoshells (AuNSs). (*a1*) A scheme of single-stranded DNA-modified AuNSs containing a spherical silica core. (*a2*) Scanning electron microscope image of AuNSs. (*a3*) Extinction spectra of AuNSs (ii). (*a4*) The release profile of DNA strands from AuNSs after thermal treatment (*black squares*) and laser irradiation (*red dots*) (Reprinted with permission from ref. [191]. Copyright 2011, American Chemical Society). (**b**) GNSs as a drug cocktail to fight against cancers through NIR light irradiation. (*b1*) A scheme of GNSs with a silica nanorattle core (GSNs) and a targeting ligand-modified surface. (*b2*) Temperature imaging of a tumor-bearing nude mouse after injection with pGSNs-Tf during photothermal therapy (2 W/cm², 3 min). (*b3*) UV-vis-NIR spectra of GSNs and PEG- and transferrin-modified GSNs (pGSNs-Tf) that indicate NPs within the inset. (*b4*) In vivo antitumor activities on MCF-7 bearing nude BALB/c mice (Reprinted with permission from ref. [134]. Copyright 2012, John Wiley & Sons, Inc.) (**c**) Au@SiO₂ as a light-mediated multifunctional theranostic platform. (*c1*) Photothermal effect of NIR irradiation (790 nm, 48 W/cm²) on the lysosomal membrane integrity. (*c2*) Intracellular localization of DOX (*red*) and Au@SiO₂ (*blue*) with Lyso-Tracker (*green*) supported by TPL images. (*c3*) Photothermal stimulus triggering DOX release for chemotherapy and the efficiency evaluated by Live-Dead assay (Reprinted with permission from

However, GNCs of several nm diameters consist of both elemental and ionic Au, but their potential toxicity or compatibility for long-term in vivo needs more attention in the future.

To study the biodistribution of Au nanoparticles in vivo, ICP-MS has been widely used to qualify the contents of Au in various organs, tissues, biological fluids, and cells. For ICP-MS determination, animals must be sacrificed to obtain a given organ to digest samples in acidic solution and to measure the Au content. To capture the nanoparticles in blood, a short half-life for clearance is a challenge using ICP-MS procedure. The optoacoustic imaging is a novel noninvasive imaging technique which provides convenience for studying real-time and semiquantitative pharmaco-kinetic and biodistribution profiles of Au nanoparticles. With a maximal absorption of NIR light, the AuNRs and Au nanostars can produce heat to ultrasound wave signals, which can be quickly visualized by multispectral optoacoustic tomography (MSOT). This technique has a high spatial resolution (150 μm for whole body; 20–50 μm for local imaging) and good contrast and provides a real-time monitoring method to collect the signals from photothermal-responsive Au nanomaterials. The contents of AuNSs and AuNRs in the blood vessels, liver, spleen, and kidneys can be sensitively detected in real time to provide the blood clearance, the accumulation, and removal process of NPs in an interested tissue or the body (Fig. 1.16). Combination of MSOT and ICP-MS is thus an appropriate approach for short- and long-term monitoring of Au nanoparticles in vivo [196].

Cells lines are widely used to study the potential toxicity and to understand mechanism. The various factors including physicochemical properties of Au nanoparticles [11], the cell culture environment [50], and cell types [56] play important roles in mediating their cellular effects. Due to the diversity of these factors, it is difficult to reveal the underlying mechanism of cytotoxicity caused by

---

Fig. 1.15 (continued) ref. [95]. Copyright 2012, John Wiley & Sons, Inc.) (**d**) DNA self-assembly on AuNRs as cancer cell-targeted and NIR light-responsive nanoparticles for thermo-chemotherapy. (*d1*) Scheme of DNA assembly and DOX loading on the AuNRs. (*d2*) Antitumor effects of various treatments on tumor-bearing mice (Reprinted with permission from ref. [192]. Copyright 2012, John Wiley & Sons, Inc.). (**e**) HAuNS-loaded microspheres (HAuNS-MSs) for thermo-chemotherapy. (*e1*) Hypothetical structures of PTX/HAuNS-MSs. (*e2*) Inhibition of U87 human gliomas growth in tumor-bearing nude mice when treated with various modes (Reprinted with permission from ref. [153]. Copyright 2010, John Wiley & Sons, Inc.). (**f**) Targeted photothermal chemotherapy using DOX-loaded HAuNSs. (*f1*) Scheme of SH-PEG-c(TNYL-RAW)-conjugated HAuNSs. (*f2*) Impact of NIR laser treatment on the growth of the bearing tumors in mice (Reprinted with permission from ref. [155]. Copyright 2012, American Association for Cancer Research). (**g**) Polymer-coated AuNCs with capability of releasing chemotherapeutic drugs controllably under NIR light irradiation. (*g1*) Scheme of polymer-coated AuNCs for drug delivery. (*g2*) Effects of nanocarriers on cell viability after treatments: (*C-1*) 2 min irradiation in absence of AuNCs; (*C-2*) 2 min irradiation in the presence of Dox-free AuNCs; and (2/5 min) 2 min or 5 min irradiation by NIR laser in presence of Dox-loaded AuNCs (Reprinted with permission from ref. [163]. Copyright 2009, Nature Publishing Group). (**h**) Enhanced release of drug from AuNCs under NIR irradiation. (*h1*) Schematic illustration of Fe_3O_4@CaP-capped AuNCs. (*h2*) Effects of dose and triggered photothermia of Fe_3O_4@CaP-capped AuNCs on viabilities of cancer cells (Reprinted with permission from ref. [165]. Copyright 2012, Royal Society of Chemistry)
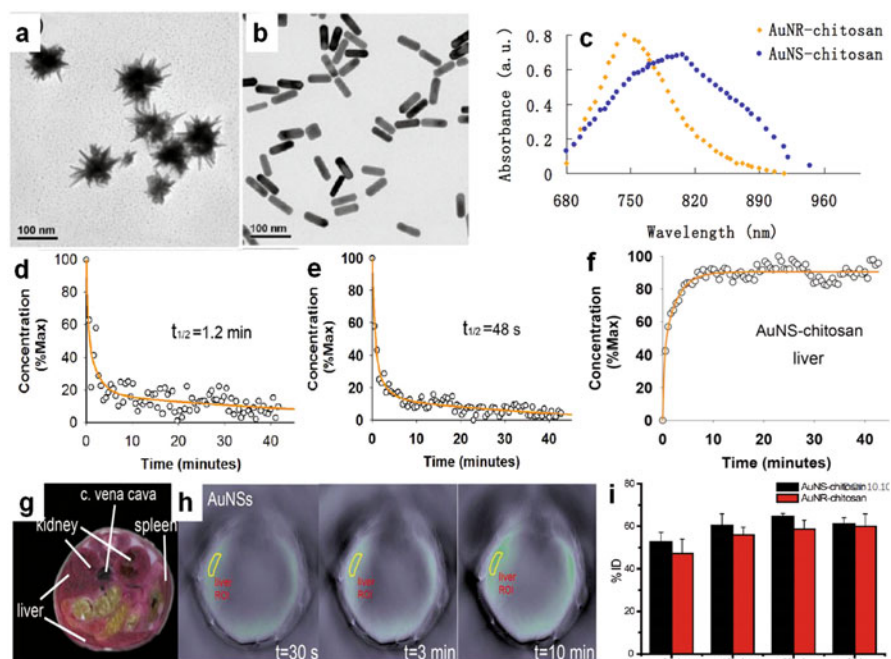
Fig. 1.16 In vivo pharmacokinetic features and biodistribution of Au nanorods and nanostars (AuNSs). (**a**, **b**) TEM images of AuNRs and AuNSs. (**c**) The vis-NIR light absorption spectra of AuNSs and AuNRs using multispectral optoacoustic tomography (MSOT). (**d**, **e**) Real-time pharmacokinetic studies of AuNSs (**d**) and AuNRs (**e**) by MSOT after injection of these Au nanoparticles into tail veins of mice. (**f**) Biodistribution and accumulation study of injected AuNSs in the liver measured by the optoacoustic signals using MSOT. (**g**) Images of a given section in the liver based on the distribution of AuNSs in a frozen section. (**h**) The real-time photoacoustic images of AuNSs at the region of interest (*ROI*, *highlighted in yellow circle*) in the liver slice. (**i**) Biodistribution of AuNSs and AuNRs in the liver, determined by ICP-MS (Reprinted with permission from ref. [196]. Copyright 2015, Royal Society of Chemistry)

Au nanoparticles. The –omics-related techniques have provided opportunity to study the induced toxicity. We thus used ^{1}H NMR spectroscopy-based metabonomics to study the pathway and to screen biomarkers of selective toxicity to cancer cells caused by CTAB-capped AuNRs. According to the results in molecular levels, normal cell lines and cancer cells show distinct changes in the metabolites that relate to oxidative stress and energy generation, the metabolism of amino acids, and nucleotides. The cellular responses are also time dependent that can illustrate how the molecular pathways contribute to distinct effects of two cell lines. The metabonomics results showed that AuNRs induce oxidative stress in both cell lines, but normal cells are more easily to offset the oxidative stress than cancer cells. Thus, the severe oxidative stress induces damage to cancer cells and to result in cell death [197]. We also employed SILAC-based proteomics to screen the signal network to inhibit the migration of cancer cells treated by AuNRs. The exposure of breast

cancer cells to AuNRs suppresses energy generation-related pathway like the mitochondrial oxidative phosphorylation (OXPHOS) and glycolysis [189]. The modulation in molecular levels helps us understand the underlying major mechanism of the cellular effects and predicts the potential risk of nanomaterials for biomedical applications.

In the end, most animal models were highly specific; thus the replicative results of biological effects and biomedical applications are sometimes hard to achieve. Predicting and evaluating toxicity of the designed Au nanostructures in vitro should base on systematic studies about how the varied factors regulate cellular effects, by combining conventional techniques for molecular and cell biology, multi-omics-based techniques, and some novel techniques in nanotoxicology. Evaluating in vivo behavior of Au nanostructures in multiple xenograft models is also necessary for clinical translation. More efforts are needed to acquire detailed information to pave the way of developing Au nanostructures for clinical applications.

References

1. Kintzel PE, Dorr RT (1995) Anticancer drug renal toxicity and elimination: dosing guidelines for altered renal function. Cancer Treat Rev 21:33–64
2. Jaracz S, Chen J, Kuznetsova LV, Ojima I (2005) Recent advances in tumor-targeting anticancer drug conjugates. Bioorg Med Chem 13:5043–5054
3. Schimmel KJ, Richel DJ, van den Brink RB, Guchelaar HJ (2004) Cardiotoxicity of cytotoxic drugs. Cancer Treat Rev 30:181–191
4. Moses MA, Brem H, Langer R (2003) Advancing the field of drug delivery: taking aim at cancer. Cancer Cell 4:337–341
5. Holohan C, Van Schaeybroeck S, Longley DB, Johnston PG (2013) Cancer drug resistance: an evolving paradigm. Nat Rev Cancer 13:714–726
6. Shimizu T, Teranishi T, Hasegawa S, Miyake M (2003) Size evolution of alkanethiol-protected gold nanoparticles by heat treatment in the solid state. J Phys Chem B 107:2719–2724
7. Liang HP, Wan LJ, Bai CL, Jiang L (2005) Gold hollow nanospheres: tunable surface plasmon resonance controlled by interior-cavity sizes. J Phys Chem B 109:7795–7800
8. Xu XD, Cortie MB (2006) Shape change and color gamut in gold nanorods, dumbbells, and dog bones. Adv Funct Mater 16:2170–2176
9. Lu XM, Au L, McLellan J, Li ZY, Marquez M, Xia YN (2007) Fabrication of cubic nanocages and nanoframes by dealloying au/ag alloy nanoboxes with an aqueous etchant based on Fe(NO$_3$)$_3$ or NH$_4$OH. Nano Lett 7:1764–1769
10. Zhang JA, Langille MR, Personick ML, Zhang K, Li SY, Mirkin CA (2010) Concave cubic gold nanocrystals with high-index facets. J Am Chem Soc 132:14012–14014

11. Qiu Y, Liu Y, Wang LM et al (2010) Surface chemistry and aspect ratio mediated cellular uptake of au nanorods. Biomaterials 31:7606–7619
12. Sun CJ, Yang H, Yuan Y et al (2011) Controlling assembly of paired gold clusters within apoferritin nanoreactor for *in vivo* kidney targeting and biomedical imaging. J Am Chem Soc 133:8617–8624
13. He WW, Liu Y, Yuan JS et al (2011) Au@Pt nanostructures as oxidase and peroxidase mimetics for use in immunoassays. Biomaterials 32:1139–1147
14. Wang LM, Lin XY, Wang J et al (2014) Novel insights into combating cancer chemotherapy resistance using a plasmonic nanocarrier: enhancing drug sensitiveness and accumulation simultaneously with localized mild photothermal stimulus of femtosecond pulsed laser. Adv Funct Mater 24:4229–4239
15. Personick ML, Langille MR, Zhang J, Harris N, Schatz GC, Mirkin CA (2011) Synthesis and isolation of {110}-faceted gold bipyramids and rhombic dodecahedra. J Am Chem Soc 133:6170–6173
16. Cheng LC, Huang JH, Chen HM et al (2012) Seedless, silver-induced synthesis of star-shaped gold/silver bimetallic nanoparticles as high efficiency photothermal therapy reagent. J Mater Chem 22:2244–2253
17. Jiang XM, Wang LM, Wang J, Chen CY (2012) Gold nanomaterials: preparation, chemical modification, biomedical applications and potential risk assessment. Appl Biochem Biotechnol 166:1533–1551
18. Cheng LC, Jiang XM, Wang J, Chen CY, Liu RS (2013) Nano-bio effects: interaction of nanomaterials with cells. Nanoscale 5:3547–3569
19. Faraday M (1857) The bakerian lecture: experimental relations of gold (and other metals) to light. Philos Trans R Soc Lond 147:145–181
20. Mie G (1908) Beitrage zur optik truber medien speziell kolloidaler metallosungen. Ann Phys 25:377–445
21. Turkevich J, Stevenson PC, Hillier J (1951) A study of the nucleation and growth processes in the synthesis of colloidal gold. Discuss Faraday Soc 11:55–75
22. Xia Y, Xiong Y, Lim B, Skrabalak SE (2009) Shape-controlled synthesis of metal nanocrystals: simple chemistry meets complex physics? Angew Chem Int Ed 48:60–103
23. Grzelczak M, Perez-Juste J, Mulvaney P, Liz-Marzan LM (2008) Shape control in gold nanoparticle synthesis. Chem Soc Rev 37:1783–1791
24. Burda C, Chen X, Narayanan R, El-Sayed MA (2005) Chemistry and properties of nanocrystals of different shapes. Chem Rev 105:1025–1102
25. Skrabalak SE, Chen J, Au L, Lu X, Li X, Xia YN (2007) Gold nanocages for biomedical applications. Adv Mater 19:3177–3184
26. Lal S, Clare SE, Halas NJ (2008) Nanoshell-enabled photothermal cancer therapy: impending clinical impact. Acc Chem Res 41:1842–1851
27. Murphy CJ, Gole AM, Stone JW et al (2008) Gold nanoparticles in biology: beyond toxicity to cellular imaging. Acc Chem Res 41:1721–1730
28. Rosi NL, Mirkin CA (2005) Nanostructures in biodiagnostics. Chem Rev 105:1547–1562
29. Lee KS, El-Sayed MA (2006) Gold and silver nanoparticles in sensing and imaging: sensitivity of plasmon response to size, shape, and metal composition. J Phys Chem B 110:19220–19225
30. Link S, El-Sayed MA (2000) Shape and size dependence of radiative, non-radiative and photothermal properties of gold nanocrystals. Int Rev Phys Chem 19:409–453
31. Hu M, Chen J, Li ZY et al (2006) Gold nanostructures: engineering their plasmonic properties for biomedical applications. Chem Soc Rev 35:1084–1094
32. Haes AJ, Stuart DA, Nie S, Van Duyne RP (2004) Using solution-phase nanoparticles, surface-confined nanoparticle arrays and single nanoparticles as biological sensing platforms. J Fluoresc 14:355–367
33. Austin LA, Mackey MA, Dreaden EC, El-Sayed MA (2014) The optical, photothermal, and facile surface chemical properties of gold and silver nanoparticles in biodiagnostics, therapy, and drug delivery. Arch Toxicol 88:1391–1417

34. Nie X, Chen CY (2012) Au nanostructures: an emerging prospect in cancer theranostics. Sci China Life Sci 55:872–883
35. Jain PK, Huang X, El-Sayed IH, El-Sayed MA (2008) Noble metals on the nanoscale: optical and photothermal properties and some applications in imaging, sensing, biology, and medicine. Acc Chem Res 41:1578–1586
36. Jain PK, Huang X, El-Sayed IH, El-Sayad MA (2007) Review of some interesting surface plasmon resonance-enhanced properties of noble metal nanoparticles and their applications to biosystems. Plasmonics 2:107–118
37. Yguerabide J, Yguerabide EE (1998) Light-scattering submicroscopic particles as highly fluorescent analogs and their use as tracer labels in clinical and biological applications: I. Theory. Anal Biochem 262:137–156
38. Jain PK, Lee KS, El-Sayed IH, El-Sayed MA (2006) Calculated absorption and scattering properties of gold nanoparticles of different size, shape, and composition: applications in biological imaging and biomedicine. J Phys Chem B 110:7238–7248
39. Sokolov K, Follen M, Aaron J et al (2003) Real-time vital optical imaging of precancer using anti-epidermal growth factor receptor antibodies conjugated to gold nanoparticles. Cancer Res 63:1999–2004
40. El-Sayed IH, Huang XH, El-Sayed MA (2005) Surface plasmon resonance scattering and absorption of anti-EGFR antibody conjugated gold nanoparticles in cancer diagnostics: applications in oral cancer. Nano Lett 5:829–834
41. Qian W, Huang XH, Kang B, El-Sayed MA (2010) Dark-field light scattering imaging of living cancer cell component from birth through division using bioconjugated gold nanoprobes. J Biomed Opt 15:046025-1-9
42. Eghtedari M, Liopo AV, Copland JA, Oraevslty AA, Motamedi M (2009) Engineering of hetero-functional gold nanorods for the *in vivo* molecular targeting of breast cancer cells. Nano Lett 9:287–291
43. Hu R, Yong KT, Roy I, Ding H, He S, Prasad PN (2009) Metallic nanostructures as localized plasmon resonance enhanced scattering probes for multiplex dark-field targeted imaging of cancer cells. J Phys Chem C 113:2676–2684
44. Huang XH, El-Sayed IH, Qian W, El-Sayed MA (2006) Cancer cell imaging and photothermal therapy in the near-infrared region by using gold nanorods. J Am Chem Soc 128:2115–2120
45. Oyelere AK, Chen PC, Huang XH, El-Sayed IH, El-Sayed MA (2007) Peptide-conjugated gold nanorods for nuclear targeting. Bioconjug Chem 18:1490–1497
46. Ding H, Yong KT, Roy I et al (2007) Gold nanorods coated with multilayer polyelectrolyte as contrast agents for multimodal imaging. J Phys Chem C 111:12552–12557
47. Kang B, Mackey MA, El-Sayed MA (2010) Nuclear targeting of gold nanoparticles in cancer cells induces DNA damage, causing cytokinesis arrest and apoptosis. J Am Chem Soc 132:1517–1519
48. Tong L, Wei QS, Wei A, Cheng JX (2009) Gold nanorods as contrast agents for biological imaging: optical properties, surface conjugation and photothermal effects. Photochem Photobiol 85:21–32
49. Park J, Estrada A, Sharp K et al (2008) Two-photon-induced photoluminescence imaging of tumors using near-infrared excited gold nanoshells. Opt Express 16:1590–1599
50. Maiorano G, Sabella S, Sorce B et al (2010) Effects of cell culture media on the dynamic formation of protein-nanoparticle complexes and influence on the cellular response. ACS Nano 4:7481–7491
51. Durr NJ, Larson T, Smith DK, Korgel BA, Sokolov K, Ben-Yakar A (2007) Two-photon luminescence imaging of cancer cells using molecularly targeted gold nanorods. Nano Lett 7:941–945
52. Puvanakrishnan P, Diagaradjane P, Kazmi SMS, Dunn AK, Krishnan S, Tunnell JW (2012) Narrow band imaging of squamous cell carcinoma tumors using topically delivered anti-EGFR antibody conjugated gold nanorods. Lasers Surg Med 44:310–317

53. Tong L, Zhao Y, Huff TB, Hansen MN, Wei A, Cheng JX (2007) Gold nanorods mediate tumor cell death by compromising membrane integrity. Adv Mater 19:3136–3141
54. Charan S, Sanjiv K, Singh N et al (2012) Development of chitosan oligosaccharide-modified gold nanorods for *in vivo* targeted delivery and noninvasive imaging by NIR irradiation. Bioconjug Chem 23:2173–2182
55. Zhang YA, Yu J, Birch DJS, Chen Y (2010) Gold nanorods for fluorescence lifetime imaging in biology. J Biomed Opt 15:020504
56. Wang LM, Liu Y, Li W et al (2011) Selective targeting of gold nanorods at the mitochondria of cancer cells: implications for cancer therapy. Nano Lett 11:772–780
57. Yuan HK, Khoury CG, Hwang H, Wilson CM, Grant GA, Vo-Dinh T (2012) Gold nanostars: surfactant-free synthesis, 3D modelling, and two-photon photoluminescence imaging. Nanotechnology 23:075102
58. Park J, Estrada A, Schwartz JA et al (2010) Intra-organ biodistribution of gold nanoparticles using intrinsic two-photon-induced photoluminescence. Lasers Surg Med 42:630–639
59. Wang YC, Xu JB, Xia XH et al (2012) Sv119-gold nanocage conjugates: a new platform for targeting cancer cells *via* sigma-2 receptors. Nanoscale 4:421–424
60. Gao L, Vadakkan TJ, Nammalvar V (2011) Nanoshells for *in vivo* imaging using two-photon excitation microscopy. Nanotechnology 22:365102
61. Au L, Zhang Q, Cobley CM et al (2010) Quantifying the cellular uptake of antibody-conjugated au nanocages by two-photon microscopy and inductively coupled plasma mass spectrometry. ACS Nano 4:35–42
62. Yuan Z, Wu CF, Zhao HZ, Jiang HB (2005) Imaging of small nanoparticle-containing objects by finite-element-based photoacoustic tomography. Opt Lett 30:3054–3056
63. Li PC, Huang SW, Wei CW, Chiou YC, Chen CD, Wang CRC (2005) Photoacoustic flow measurements by use of laser-induced shape transitions of gold nanorods. Opt Lett 30:3341–3343
64. Wang YW, Xie XY, Wang XD et al (2004) Photoacoustic tomography of a nanoshell contrast agent in the *in vivo* rat brain. Nano Lett 4:1689–1692
65. Mallidi S, Larson T, Tam J et al (2009) Multiwavelength photoacoustic imaging and plasmon resonance coupling of gold nanoparticles for selective detection of cancer. Nano Lett 9:2825–2831
66. Kim C, Cho EC, Chen JY et al (2010) *In vivo* molecular photoacoustic tomography of melanomas targeted by bioconjugated gold nanocages. ACS Nano 4:4559–4564
67. Cai X, Li WY, Kim CH, Yuan YC, Wang LHV, Xia YN (2011) *In vivo* quantitative evaluation of the transport kinetics of gold nanocages in a lymphatic system by noninvasive photoacoustic tomography. ACS Nano 5:9658–9667
68. Li PC, Wang CRC, Shieh DB et al (2008) *In vivo* photoacoustic molecular imaging with simultaneous multiple selective targeting using antibody-conjugated gold nanorods. Opt Express 16:18605–18615
69. Yang SH, Ye F, Xing D (2012) Intracellular label-free gold nanorods imaging with photoacoustic microscopy. Opt Express 20:10370–10375
70. Jokerst JV, Thangaraj M, Kempen PJ, Sinclair R, Gambhir SS (2012) Photoacoustic imaging of mesenchymal stem cells in living mice via silica-coated gold nanorods. ACS Nano 6:5920–5930
71. von Maltzahn G, Park JH, Agrawal A et al (2009) Computationally guided photothermal tumor therapy using long-circulating gold nanorod antennas. Cancer Res 69:3892–3900
72. Luo T, Huang P, Gao G et al (2011) Mesoporous silica-coated gold nanorods with embedded indocyanine green for dual mode X-ray CT and NIR fluorescence imaging. Opt Express 19:17030–17039
73. Huang P, Bao L, Zhang CL et al (2011) Folic acid-conjugated silica-modified gold nanorods for x-ray/ct imaging-guided dual-mode radiation and photo-thermal therapy. Biomaterials 32:9796–9809
74. Lozano N, Al-Jamal WT, Taruttis A et al (2012) Liposome-gold nanorod hybrids for high-resolution visualization deep in tissues. J Am Chem Soc 134:13256–13258

75. Zagaynova EV, Shirmanova MV, Kirillin MY et al (2008) Contrasting properties of gold nanoparticles for optical coherence tomography: phantom, *in vivo* studies and Monte Carlo simulation. Phys Med Biol 53:4995–5009

76. Oldenburg AL, Hansen MN, Ralston TS, Wei A, Boppart SA (2009) Imaging gold nanorods in excised human breast carcinoma by spectroscopic optical coherence tomography. J Mater Chem 19:6407–6411

77. Jung Y, Reif R, Zeng YG, Wang RK (2011) Three-dimensional high-resolution imaging of gold nanorods uptake in sentinel lymph nodes. Nano Lett 11:2938–2943

78. Kim CS, Wilder-Smith P, Ahn YC, Liaw LHL, Chen ZP, Kwon YJ (2009) Enhanced detection of early-stage oral cancer *in vivo* by optical coherence tomography using multimodal delivery of gold nanoparticles. J Biomed Opt 14:034008

79. Nie SM, Emery SR (1997) Probing single molecules and single nanoparticles by surface-enhanced Raman scattering. Science 275:1102–1106

80. Moskovits M (2006) Surface-enhanced Raman spectroscopy: a brief perspective. In: Kneipp K, Moskovits M, Kneipp H (eds) Surface-enhanced Raman scattering: physics and applications. Springer, Berlin\Heidelberg, pp 1–17

81. Chon H, Lee S, Son SW, Oh CH, Choo J (2009) Highly sensitive immunoassay of lung cancer marker carcinoembryonic antigen using surface-enhanced Raman scattering of hollow gold nanospheres. Anal Chem 81:3029–3034

82. Bishnoi SW, Lin YJ, Tibudan M et al (2011) SERS biodetection using gold-silica nanoshells and nitrocellulose membranes. Anal Chem 83:4053–4060

83. Wu L, Wang ZY, Zong SF et al (2013) Simultaneous evaluation of p53 and p21 expression level for early cancer diagnosis using sers technique. Analyst 138:3450–3456

84. Wang GF, Lipert RJ, Jain M et al (2011) Detection of the potential pancreatic cancer marker muc4 in serum using surface-enhanced Raman scattering. Anal Chem 83:2554–2561

85. Li M, Cushing SK, Zhang JM et al (2013) Three-dimensional hierarchical plasmonic nano-architecture enhanced surface-enhanced Raman scattering immunosensor for cancer bio-marker detection in blood plasma. ACS Nano 7:4967–4976

86. Huang XH, El-Sayed IH, Qian W, El-Sayed MA (2007) Cancer cells assemble and align gold nanorods conjugated to antibodies to produce highly enhanced, sharp, and polarized surface Raman spectra: a potential cancer diagnostic marker. Nano Lett 7:1591–1597

87. Kang B, Austin LA, El-Sayed MA (2012) Real-time molecular imaging throughout the entire cell cycle by targeted plasmonic-enhanced Rayleigh/Raman spectroscopy. Nano Lett 12:5369–5375

88. Yigit MV, Zhu LY, Ifediba MA et al (2011) Noninvasive MRI-SERS imaging in living mice using an innately bimodal nanomaterial. ACS Nano 5:1056–1066

89. Wang X, Qian XM, Beitler JJ et al (2011) Detection of circulating tumor cells in human peripheral blood using surface-enhanced Raman scattering nanoparticles. Cancer Res 71:1526–1532

90. Pitsillides CM, Joe EK, Wei XB, Anderson RR, Lin CP (2003) Selective cell targeting with light-absorbing microparticles and nanoparticles. Biophys J 84:4023–4032

91. El-Sayed IH, Huang XH, El-Sayed MA (2006) Selective laser photo-thermal therapy of epithelial carcinoma using anti-egfr antibody conjugated gold nanoparticles. Cancer Lett 239:129–135

92. Rejiya CS, Kumar J, Raji V, Vibin M, Abraham A (2012) Laser immunotherapy with gold nanorods causes selective killing of tumour cells. Pharmacol Res 65:261–269

93. Dickerson EB, Dreaden EC, Huang XH et al (2008) Gold nanorod assisted near-infrared plasmonic photothermal therapy (pptt) of squamous cell carcinoma in mice. Cancer Lett 269:57–66

94. Li ZM, Huang P, Zhang XJ et al (2010) RGD-conjugated dendrimer-modified gold nanorods for *in vivo* tumor targeting and photothermal therapy. Mol Pharm 7:94–104

95. Zhang ZJ, Wang LM, Wang J et al (2012) Mesoporous silica-coated gold nanorods as a light-mediated multifunctional theranostic platform for cancer treatment. Adv Mater 24:1418–1423

96. Guo LH, Xu Y, Ferhan AR, Chen GN, Kim DH (2013) Oriented gold nanoparticle aggregation for colorimetric sensors with surprisingly high analytical figures of merit. J Am Chem Soc 135:12338–12345
97. Hirsch LR, Stafford RJ, Bankson JA et al (2003) Nanoshell-mediated near-infrared thermal therapy of tumors under magnetic resonance guidance. Proc Natl Acad Sci U S A 100:13549–13554
98. Bernardi RJ, Lowery AR, Thompson PA, Blaney SM, West JL (2008) Immunonanoshells for targeted photothermal ablation in medulloblastoma and glioma: an *in vitro* evaluation using human cell lines. J Neurooncol 86:165–172
99. Day ES, Thompson PA, Zhang LN et al (2011) Nanoshell-mediated photothermal therapy improves survival in a murine glioma model. J Neurooncol 104:55–63
100. Diagaradjane P, Shetty A, Wang JC et al (2008) Modulation of *in vivo* tumor radiation response via gold nanoshell-mediated vascular-focused hyperthermia: characterizing an integrated antihypoxic and localized vascular disrupting targeting strategy. Nano Lett 8:1492–1500
101. McIntosh CM, Esposito EA, Boal AK, Simard JM, Martin CT, Rotello VM (2001) Inhibition of DNA transcription using cationic mixed monolayer protected gold clusters. J Am Chem Soc 123:7626–7629
102. Alkilany AM, Thompson LB, Boulos SP, Sisco PN, Murphy CJ (2012) Gold nanorods: their potential for photothermal therapeutics and drug delivery, tempered by the complexity of their biological interactions. Adv Drug Deliv Rev 64:190–199
103. Park H, Lee S, Chen L et al (2009) SERS imaging of Her2-overexpressed MCF-7 cells using antibody-conjugated gold nanorods. Phys Chem Chem Phys 11:7444–7449
104. Wang LM, Li JY, Pan J et al (2013) Revealing the binding structure of the protein corona on gold nanorods using synchrotron radiation-based techniques: understanding the reduced damage in cell membranes. J Am Chem Soc 135:17359–17368
105. Wang L, Jiang X, Ji Y et al (2013) Surface chemistry of gold nanorods: origin of cell membrane damage and cytotoxicity. Nanoscale 5:8384–8391
106. Kim CK, Ghosh P, Pagliuca C, Zhu ZJ, Menichetti S, Rotello VM (2009) Entrapment of hydrophobic drugs in nanoparticle monolayers with efficient release into cancer cells. J Am Chem Soc 131:1360–1361
107. Gorelikov I, Matsuura N (2008) Single-step coating of mesoporous silica on cetyltrimethyl ammonium bromide-capped nanoparticles. Nano Lett 8:369–373
108. Slowing II, Vivero-Escoto JL, Wu CW, Lin VSY (2008) Mesoporous silica nanoparticles as controlled release drug delivery and gene transfection carriers. Adv Drug Deliv Rev 60:1278–1288
109. Zhang ZJ, Wang J, Nie X et al (2014) Near infrared laser-induced targeted cancer therapy using thermoresponsive polymer encapsulated gold nanorods. J Am Chem Soc 136:7317–7326
110. Amoozgar Z, Yeo Y (2012) Recent advances in stealth coating of nanoparticle drug delivery systems. WIRES Nanomed Nanobiotechnol 4:219–233
111. Wang J, Byrne JD, Napier ME, DeSimone JM (2011) More effective nanomedicines through particle design. Small 7:1919–1931
112. Alivisatos AP, Johnsson KP, Peng XG et al (1996) Organization of 'nanocrystal molecules' using DNA. Nature 382:609–611
113. Mirkin CA, Letsinger RL, Mucic RC, Storhoff JJ (1996) A DNA-based method for rationally assembling nanoparticles into macroscopic materials. Nature 382:607–609
114. Glynou K, Ioannou PC, Christopoulos TK, Syriopoulou V (2003) Oligonucleotide-functionalized gold nanoparticles as probes in a dry-reagent strip biosensor for DNA analysis by hybridization. Anal Chem 75:4155–4160
115. Lee JS, Han MS, Mirkin CA (2007) Colorimetric detection of mercuric ion (Hg^{2+}) in aqueous media using DNA-functionalized gold nanoparticles. Angew Chem Int Ed 46:4093–4096

116. Rosi NL, Giljohann DA, Thaxton CS, Lytton-Jean AK, Han MS, Mirkin CA (2006) Oligonucleotide-modified gold nanoparticles for intracellular gene regulation. Science 312:1027–1030

117. Austin LA, Kang B, Yen CW, El-Sayed MA (2011) Nuclear targeted silver nanospheres perturb the cancer cell cycle differently than those of nanogold. Bioconjug Chem 22:2324–2331

118. Xiao YL, Hong H, Matson VZ et al (2012) Gold nanorods conjugated with doxorubicin and crgd for combined anticancer drug delivery and pet imaging. Theranostics 2:757–768

119. Black KC, Kirkpatrick ND, Troutman TS et al (2008) Gold nanorods targeted to delta opioid receptor: plasmon-resonant contrast and photothermal agents. Mol Imaging 7:50–57

120. Yamashita S, Fukushima H, Akiyama Y et al (2011) Controlled-release system of single-stranded DNA triggered by the photothermal effect of gold nanorods and its *in vivo* application. Bioorg Med Chem 19:2130–2135

121. Lundqvist M, Stigler J, Elia G, Lynch I, Cedervall T, Dawson KA (2008) Nanoparticle size and surface properties determine the protein corona with possible implications for biological impacts. Proc Natl Acad Sci U S A 105:14265–14270

122. Prabaharan M, Grailer JJ, Pilla S, Steeber DA, Gong SQ (2009) Gold nanoparticles with a monolayer of doxorubicin-conjugated amphiphilic block copolymer for tumor-targeted drug delivery. Biomaterials 30:6065–6075

123. Qian XM, Peng XH, Ansari DO et al (2008) *In vivo* tumor targeting and spectroscopic detection with surface-enhanced Raman nanoparticle tags. Nat Biotechnol 26:83–90

124. Fischler M, Sologubenko A, Mayer J et al (2008) Chain-like assembly of gold nanoparticles on artificial DNA templates *via* 'click chemistry'. Chem Commun 2:169–171

125. Zhu K, Zhang Y, He S et al (2012) Quantification of proteins by functionalized gold nanoparticles using click chemistry. Anal Chem 84:4267–4270

126. Loo C, Lin A, Hirsch L et al (2004) Nanoshell-enabled photonics-based imaging and therapy of cancer. Technol Cancer Res Treat 3:33–40

127. Loo C, Lowery A, Halas NJ, West J, Drezek R (2005) Immunotargeted nanoshells for integrated cancer imaging and therapy. Nano Lett 5:709–711

128. Gobin AM, Lee MH, Halas NJ, James WD, Drezek RA, West JL (2007) Near-infrared resonant nanoshells for combined optical imaging and photothermal cancer therapy. Nano Lett 7:1929–1934

129. Lu W, Melancon MP, Xiong CY et al (2011) Effects of photoacoustic imaging and photothermal ablation therapy mediated by targeted hollow gold nanospheres in an orthotopic mouse xenograft model of glioma. Cancer Res 71:6116–6121

130. Bardhan R, Chen WX, Perez-Torres C et al (2009) Nanoshells with targeted simultaneous enhancement of magnetic and optical imaging and photothermal therapeutic response. Adv Funct Mater 19:3901–3909

131. Chen WX, Bardhan R, Bartels M et al (2010) A molecularly targeted theranostic probe for ovarian cancer. Mol Cancer Ther 9:1028–1038

132. Bardhan R, Chen WX, Bartels M et al (2010) Tracking of multimodal therapeutic nanocomplexes targeting breast cancer *in vivo*. Nano Lett 10:4920–4928

133. Liu HY, Chen D, Li LL et al (2011) Multifunctional gold nanoshells on silica nanorattles: a platform for the combination of photothermal therapy and chemotherapy with low systemic toxicity. Angew Chem Int Ed 50:891–895

134. Liu HY, Liu TL, Wu XL et al (2012) Targeting gold nanoshells on silica nanorattles: a drug cocktail to fight breast tumors via a single irradiation with near-infrared laser light. Adv Mater 24:755–761

135. Lee SM, Park H, Yoo KH (2010) Synergistic cancer therapeutic effects of locally delivered drug and heat using multifunctional nanoparticles. Adv Mater 22:4049–4053

136. Xie HA, Diagaradjane P, Deorukhkar AA et al (2011) Integrin alpha(v) beta(3)-targeted gold nanoshells augment tumor vasculature-specific imaging and therapy. Int J Nanomedicine 6:259–269

137. Melancon MP, Elliott A, Ji XJ et al (2011) Theranostics with multifunctional magnetic gold nanoshells photothermal therapy and T2 magnetic resonance imaging. Invest Radiol 46:132–140
138. Ke HT, Wang JR, Dai ZF et al (2011) Gold-nanoshelled microcapsules: a theranostic agent for ultrasound contrast imaging and photothermal therapy. Angew Chem Int Ed 50:3017–3021
139. Ma Y, Liang XL, Tong S, Bao G, Ren QS, Dai ZF (2013) Gold nanoshell nanomicelles for potential magnetic resonance imaging, light-triggered drug release, and photothermal therapy. Adv Funct Mater 23:815–822
140. Choi J, Yang J, Jang E et al (2011) Gold nanostructures as photothermal therapy agent for cancer. Anti Cancer Agents Med 11:953–964
141. Huff TB, Tong L, Zhao Y, Hansen MN, Cheng JX, Wei A (2007) Hyperthermic effects of gold nanorods on tumor cells. Nanomedicine 2:125–132
142. Yi DK, Sun IC, Ryu JH et al (2010) Matrix metalloproteinase sensitive gold nanorod for simultaneous bioimaging and photothermal therapy of cancer. Bioconjug Chem 21:2173–2177
143. Choi J, Yang J, Bang D et al (2012) Targetable gold nanorods for epithelial cancer therapy guided by near-IR absorption imaging. Small 8:746–753
144. Kuo WS, Chang CN, Chang YT et al (2010) Gold nanorods in photodynamic therapy, as hyperthermia agents, and in near-infrared optical imaging. Angew Chem Int Ed 49:2711–2715
145. Jang B, Park JY, Tung CH, Kim IH, Choi Y (2011) Gold nanorod-photosensitizer complex for near-infrared fluorescence imaging and photodynamic/photothermal therapy in vivo. ACS Nano 5:1086–1094
146. Zhang Y, Qian J, Wang D, Wang YL, He SL (2013) Multifunctional gold nanorods with ultrahigh stability and tunability for in vivo fluorescence imaging, sers detection, and photodynamic therapy. Angew Chem Int Ed 52:1148–1151
147. Zhang ZJ, Wang J, Chen CY (2013) Near-infrared light-mediated nanoplatforms for cancer thermo-chemotherapy and optical imaging. Adv Mater 25:3869–3880
148. Zhang ZJ, Wang J, Chen CY (2013) Gold nanorods based platforms for light-mediated theranostics. Theranostics 3:223–238
149. Guo R, Zhang L, Qian H, Li R, Jiang X, Liu B (2010) Multifunctional nanocarriers for cell imaging, drug delivery, and near-IR photothermal therapy. Langmuir 26:5428–5434
150. Melancon MP, Lu W, Yang Z et al (2008) In vitro and in vivo targeting of hollow gold nanoshells directed at epidermal growth factor receptor for photothermal ablation therapy. Mol Cancer Ther 7:1730–1739
151. Lu W, Xiong CY, Zhang GD et al (2009) Targeted photothermal ablation of murine melanomas with melanocyte-stimulating hormone analog-conjugated hollow gold nanospheres. Clin Cancer Res 15:876–886
152. Lu W, Zhang GD, Zhang R et al (2010) Tumor site-specific silencing of NF-kappa b p65 by targeted hollow gold nanosphere-mediated photothermal transfection. Cancer Res 70:3177–3188
153. You J, Shao RP, Wei X, Gupta S, Li C (2010) Near-infrared light triggers release of paclitaxel from biodegradable microspheres: photothermal effect and enhanced antitumor activity. Small 6:1022–1031
154. You J, Zhang GD, Li C (2010) Exceptionally high payload of doxorubicin in hollow gold nanospheres for near-infrared light-triggered drug release. ACS Nano 4:1033–1041
155. You J, Zhang R, Xiong CY et al (2012) Effective photothermal chemotherapy using doxorubicin-loaded gold nanospheres that target Ephb4 receptors in tumors. Cancer Res 72:4777–4786
156. You J, Zhang R, Zhang GD et al (2012) Photothermal-chemotherapy with doxorubicin-loaded hollow gold nanospheres: a platform for near-infrared light-trigged drug release. J Control Release 158:319–328

157. Melancon MP, Elliott AM, Shetty A, Huang Q, Stafford RJ, Li C (2011) Near-infrared light modulated photothermal effect increases vascular perfusion and enhances polymeric drug delivery. J Control Release 156:265–272

158. Sun YG, Mayers BT, Xia YN (2002) Template-engaged replacement reaction: a one-step approach to the large-scale synthesis of metal nanostructures with hollow interiors. Nano Lett 2:481–485

159. Chen JY, Yang MX, Zhang QA et al (2010) Gold nanocages: a novel class of multifunctional nanomaterials for theranostic applications. Adv Funct Mater 20:3684–3694

160. Chen JY, Wang DL, Xi JF et al (2007) Immuno gold nanocages with tailored optical properties for targeted photothermal destruction of cancer cells. Nano Lett 7:1318–1322

161. Au L, Zheng DS, Zhou F, Li ZY, Li XD, Xia YN (2008) A quantitative study on the photothermal effect of immuno gold nanocages targeted to breast cancer cells. ACS Nano 2:1645–1652

162. Chen JY, Glaus C, Laforest R et al (2010) Gold nanocages as photothermal transducers for cancer treatment. Small 6:811–817

163. Yavuz MS, Cheng YY, Chen JY et al (2009) Gold nanocages covered by smart polymers for controlled release with near-infrared light. Nat Mater 8:935–939

164. Moon GD, Choi SW, Cai X et al (2011) A new theranostic system based on gold nanocages and phase-change materials with unique features for photoacoustic imaging and controlled release. J Am Chem Soc 133:4762–4765

165. Shi P, Qu KG, Wang JS, Li M, Ren JS, Qu XG (2012) Ph-responsive nir enhanced drug release from gold nanocages possesses high potency against cancer cells. Chem Commun 48:7640–7642

166. Yuan H, Fales AM, Vo-Dinh T (2012) Tat peptide-functionalized gold nanostars: enhanced intracellular delivery and efficient nir photothermal therapy using ultralow irradiance. J Am Chem Soc 134:11358–11361

167. Yuan HK, Khoury CG, Wilson CM, Grant GA, Bennett AJ, Vo-Dinh T (2012) *In vivo* particle tracking and photothermal ablation using plasmon-resonant gold nanostars. Nanomedicine Nanotechnol 8:1355–1363

168. Wang SJ, Huang P, Nie LM et al (2013) Single continuous wave laser induced photodynamic/plasmonic photothermal therapy using photosensitizer-functionalized gold nanostars. Adv Mater 25:3055–3061

169. Lapotko DO (2006) Laser-induced bubbles in living cells. Lasers Surg Med 38:240–248

170. Wagner DS, Delk NA, Lukianova-Hleb EY, Hafner JH, Farach-Carson MC, Lapotko DO (2010) The *in vivo* performance of plasmonic nanobubbles as cell theranostic agents in zebrafish hosting prostate cancer xenografts. Biomaterials 31:7567–7574

171. Lukianova-Hleb EY, Lapotko DO (2014) Nano-theranostics with plasmonic nanobubbles. IEEE J Sel Top Quantum 20:163–174

172. Lukianova-Hleb EY, Oginsky AO, Samaniego AP et al (2011) Tunable plasmonic nanoprobes for theranostics of prostate cancer. Theranostics 1:3–17

173. Lukianova-Hleb EY, Ren XY, Zasadzinski JA, Wu XW, Lapotko DO (2012) Plasmonic nanobubbles enhance efficacy and selectivity of chemotherapy against drug-resistant cancer cells. Adv Mater 24:3831–3837

174. Lukianova-Hleb EY, Samaniego AP, Wen JG, Metelitsa LS, Chang CC, Lapotko DO (2011) Selective gene transfection of individual cells *in vitro* with plasmonic nanobubbles. J Control Release 152:286–293

175. Hu J, Zhu XL, Li H et al (2014) Theranostic au cubic nano-aggregates as potential photoacoustic contrast and photothermal therapeutic agents. Theranostics 4:534–545

176. Ma LL, Feldman MD, Tam JM et al (2009) Small multifunctional nanoclusters (nanoroses) for targeted cellular imaging and therapy. ACS Nano 3:2686–2696

177. Kim D, Park S, Lee JH, Jeong YY, Jon S (2007) Antibiofouling polymer-coated gold nanoparticles as a contrast agent for *in vivo* X-ray computed tomography imaging. J Am Chem Soc 129:7661–7665

178. Kim D, Jeong YY, Jon S (2010) A drug-loaded aptamer-gold nanoparticle bioconjugate for combined ct imaging and therapy of prostate cancer. ACS Nano 4:3689–3696
179. Zhou HS, Honma I, Komiyama H, Haus JW (1994) Controlled synthesis and quantum-size effect in gold-coated nanoparticles. Phys Rev B 50:12052–12056
180. Averitt RD, Sarkar D, Halas NJ (1997) Plasmon resonance shifts of au-coated au2s nanoshells: insight into multicomponent nanoparticle growth. Phys Rev Lett 78:4217–4220
181. Decuzzi P, Lee S, Bhushan B, Ferrari M (2005) A theoretical model for the margination of particles within blood vessels. Ann Biomed Eng 33:179–190
182. Chithrani BD, Ghazani AA, Chan WCW (2006) Determining the size and shape dependence of gold nanoparticle uptake into mammalian cells. Nano Lett 6:662–668
183. Day ES, Bickford LR, Slater JH, Riggall NS, Drezek RA, West JL (2010) Antibody-conjugated gold-gold sulfide nanoparticles as multifunctional agents for imaging and therapy of breast cancer. Int J Nanomedicine 5:445–454
184. Gobin AM, Watkins EM, Quevedo E, Colvin VL, West JL (2010) Near-infrared-resonant gold/gold sulfide nanoparticles as a photothermal cancer therapeutic agent. Small 6:745–752
185. Gao L, Liu R, Gao FP, Wang YL, Jiang XL, Gao XY (2014) Plasmon-mediated generation of reactive oxygen species from near-infrared light excited gold nanocages for photodynamic therapy *in vitro*. ACS Nano 8:7260–7271
186. Yy L, Wen T, Zhao RF et al (2014) Localized electric field of plasmonic nanoplatform enhanced photodynamic tumor therapy. ACS Nano 8:11529–11542
187. Trachootham D, Alexandre J, Huang P (2009) Targeting cancer cells by ros-mediated mechanisms: a radical therapeutic approach? Nat Rev Drug Discov 8:579–591
188. Xu YY, Wang J, Li XF et al (2014) Selective inhibition of breast cancer stem cells by gold nanorods mediated plasmonic hyperthermia. Biomaterials 35:4667–4677
189. Zhou T, Yu M, Zhang B et al (2014) Inhibition of cancer cell migration by gold nanorods: molecular mechanisms and implications for cancer therapy. Adv Funct Mater 24:6922–6932
190. Weintraub K (2013) Biomedicine: the new gold standard. Nature 495:S14–S16
191. Huschka R, Zuloaga J, Knight MW, Brown LV, Nordlander P, Halas NJ (2011) Light-induced release of DNA from gold nanoparticles: nanoshells and nanorods. J Am Chem Soc 133:12247–12255
192. Xiao ZY, Ji CW, Shi JJ et al (2012) DNA self-assembly of targeted near-infrared-responsive gold nanoparticles for cancer thermo-chemotherapy. Angew Chem Int Ed 51:11853–11857
193. Khlebtsov N, Dykman L (2011) Biodistribution and toxicity of engineered gold nanoparticles: a review of *in vitro* and *in vivo* studies. Chem Soc Rev 40:1647–1671
194. Zhang JJ, Nie X, Ji YL et al (2013) Quantitative biokinetics and systemic translocation of various gold nanostructures are highly dependent on their size and shape. J Nanosci Nanotechnol 13:1–15
195. Wang LM, Li YF, Zhou LJ et al (2010) Characterization of gold nanorods *in vivo* by integrated analytical techniques: their uptake, retention, and chemical forms. Anal Bioanal Chem 396:1105–1114
196. Wang J, Xie YD, Wang LM et al (2015) *In vivo* pharmacokinetic features and biodistribution of star and rod shaped gold nanoparticles by multispectral optoacoustic tomography. RSC Adv 5:7529–7538
197. Zhang LM, Wang LM, Hu YL et al (2013) Selective metabolic effects of gold nanorods on normal and cancer cells and their application in anticancer drug screening. Biomaterials 34:7117–7126